

Implicit Third-Order Peer Triplets with Variable Stepsizes for Gradient-Based Solutions in Large-Scale ODE-Constrained Optimal Control

Jens Lang

Technical University Darmstadt, Department of Mathematics

Dolivostraße 15, 64293 Darmstadt, Germany

lang@mathematik.tu-darmstadt.de

Bernhard A. Schmitt

Philipps-Universität Marburg, Department of Mathematics,

Hans-Meerwein-Straße 6, 35043 Marburg, Germany

schmitt@mathematik.uni-marburg.de

September 16, 2025

Abstract

This paper is concerned with the theory, construction and application of variable-stepsize implicit Peer two-step methods that are super-convergent for variable stepsizes, i.e., preserve their classical order achieved for uniform stepsizes when applied in a gradient-based solution algorithm to solve ODE-constrained optimal control problems in a first-discretize-then-optimize setting. Gradients of the objective function can be computed most efficiently using approximate adjoint variables. High accuracy with moderate computational effort can be achieved through time integration methods that satisfy a sufficiently large number of adjoint order conditions for variable stepsizes and provide gradients with higher-order consistency. In this paper, we enhance our previously developed variable implicit two-step Peer triplets constructed in [J. Comput. Appl. Math. 460, 2025] to get ready for large-scale dynamical systems with varying time scales without loosing efficiency. A key advantage of Peer methods is their use of multiple stages with the same high stage order, which prevents order reduction — an issue commonly encountered in semi-discretized PDE problems with boundary control. Two third-order methods with four stages, good stability properties, small error constants, and a grid adaptation by equi-distributing global errors are constructed and tested for a 1D boundary heat control problem and an optimal control of cytotoxic therapies in the treatment of prostate cancer.

Key words. Implicit Peer two-step methods, nonlinear optimal control, gradient-based optimization, first-discretize-then-optimize, discrete adjoints, variable stepsizes

1 Introduction

Recently, we have developed and tested third- and fourth-order implicit Peer two-step methods [15, 16, 17, 18, 19] to solve ODE-constrained optimal control problems of the form

$$\text{minimize } \mathcal{C}(y(T)) \quad (1)$$

$$\text{subject to } y'(t) = f(y(t), u(t)), \quad u(t) \in U_{ad}, \quad t \in (0, T], \quad (2)$$

$$y(0) = y_0, \quad (3)$$

with the state $y(t) \in \mathbb{R}^m$, the control $u(t) \in \mathbb{R}^d$, $f : \mathbb{R}^m \times \mathbb{R}^d \mapsto \mathbb{R}^m$, the objective function $\mathcal{C} : \mathbb{R}^m \mapsto \mathbb{R}$, where the set of admissible controls $U_{ad} \subset \mathbb{R}^d$ is closed and convex. The Mayer form $\mathcal{C}(y(T))$ of the objective function which only considers state values at $t = T$ is quite general. For example, terms given in the Lagrange form

$$\mathcal{C}_L(y, u) := \int_0^T l(y(t), u(t)) dt \quad (4)$$

can be equivalently transferred to the Mayer form by adding a new differential equation $y'_{m+1}(t) = l(y(t), u(t))$ and initial values $y_{m+1}(0) = 0$ to the constraints. Then (4) simply reduces to $y_{m+1}(T)$.

The design of efficient time integrators for the numerical solution of such problems with large m arising from semi-discretized time-dependent partial differential equations is still of great interest since difficulties arise through additional adjoint order conditions, some recent literature is [1, 2]. Implicit Peer two-step methods overcome the structural disadvantages of one-step and multi-step methods such as symplectic or generalized partitioned Runge-Kutta methods [5, 12, 21] and backward differentiation formulas [4]. They avoid order reduction of one-step methods, e.g., for boundary control problems of PDEs [17], and have good stability properties. Peer methods also allow the approximation of adjoints in a first-discretize-then-optimize (FDTO) approach with higher order, which still seems to be an unsolved problem for multi-step methods. FDTO is the most commonly used method and possesses the advantage of providing consistent gradients for state-of-the-art optimization algorithms. We refer the reader to the detailed discussions in our previous papers [15, 16, 17, 18, 19].

So far we have considered the use of 4-stage diagonally implicit Peer two-step methods that are of order three, at least, if applied with non-uniform time grids to a reduced first-order optimality system [19]. The transition to gradient-based solution algorithms without analytic elimination of the control $u(t)$ requires additional order conditions for the control and certain positivity requirements for column sums in the matrix triplet (K_0, K, K_N) used in (5) to define the forward Peer method [18]. Starting with two positive methods from [19], we derive a third-order *flip-symmetric pulcherrima* Peer triplet which is $A(61.59^\circ)$ -stable, and a second $A(83.74^\circ)$ -stable Peer triplet with improved stability for smoothly varying grids. Symmetry plays an important role in the theory of geometric integration which has a strong link to the Hamiltonian structure of the first-order optimality system discussed in Section 3, see [11, 22]. Here, it also forms the foundation for the remarkably good performance of the pulcherrima triplet. Since the start and end method of the triplet are of one-step form, the requirement of high stage order prohibits the use of triangular coefficient matrices. However, for both methods triangular iterations are provided in these steps to avoid additional memory requirements for large nonlinear systems.

We also present a method for determining an optimized stepsize sequence *a posteriori* by using error estimators to approximate global errors and implement the error equi-distribution principle

introduced in [3, Chapter9.1.1]. Since Peer triplets retain their classical order even with variable time steps, these grid refinements can be applied without any loss of efficiency.

The paper is organized as follows. In Section 2, we introduce a generalized form of a Peer two-step triplet. The continuous and discrete first order optimality conditions are presented in Section 3. The framework of gradient-based optimization, which relies on an iterative forward-backward marching scheme, is discussed in Section 4. Several properties of Peer triplets, including the standard and boundary methods, are described in Section 5. In Section 6, we modify two of our previous Peer two-step triplets of practical interest. Grid improvement is discussed in Section 7 and numerical results are given in Section 8. Conclusions are stated in Section 9.

Throughout the paper, we use the following notations: e_i denotes a cardinal basis vector, $\mathbb{1}_k = (1, \dots, 1)^\top \in \mathbb{R}^k$ is the vector of ones, and $I_k \in \mathbb{R}^{k \times k}$ is the identity matrix. The latter two are occasionally used without index if there is no ambiguity.

2 Two-step Peer triplets

Peer two-step methods for the numerical solution of (2)–(3), which are suitable for optimal control, have the general redundant form

$$(A_n \otimes I_m) Y_n = (B_n \otimes I_m) Y_{n-1} + h_n (K_n \otimes I_m) F(Y_n, U_n), \quad n \geq 1, \quad (5)$$

where $\{t_0, t_1, \dots, t_{N+1}\} \subseteq [0, T]$ is a grid with stepsizes $h_n = t_{n+1} - t_n$, $n = 0, \dots, N$. The stage and control solutions $Y_n = (Y_{ni})_{i=1}^s \in \mathbb{R}^{sm}$ and $U_n = (U_{ni})_{i=1}^s \in \mathbb{R}^{sd}$ are approximations of $(y(t_n + c_i h_n))_{i=1}^s$ and $(u(t_n + c_i h_n))_{i=1}^s$, respectively, where all s stages have equal accuracy. Also, $F(Y_n, U_n) = (f(Y_{ni}, U_{ni}))_{i=1}^s$ is used. The equal stage order motivates the attribute *peer* and is the key for avoiding order reduction. The nodes c_1, \dots, c_s are associated with the interval $[0, 1]$ but some may lie outside. We note that (5) is a redundant form of Peer two-step methods and may be simplified, e.g., by setting $K_n \equiv I$. However, we will see below that the coefficient matrix K leads to additional degrees of freedom when considering *adjoint* Peer methods.

An exceptional, Runge-Kutta-like starting step is used,

$$(A_0 \otimes I_m) Y_0 = a \otimes y_0 + h_0 (K_0 \otimes I_m) F(Y_0, U_0),$$

with $a \in \mathbb{R}^s$. With variable stepsizes, we employ as in [19] one *standard Peer method* (A, K, B_n) for the time steps with $1 \leq n < N$, where $A \in \mathbb{R}^{s \times s}$ is a fixed nonsingular lower triangular matrix and $K \in \mathbb{R}^{s \times s}$ is a fixed diagonal matrix with strictly positive entries in order to restrict the size of the stage equations to m unknowns. The matrix B_n will only depend on the current stepsize ratio $\sigma_n = h_n/h_{n-1}$ in the form $B_n = B(\sigma_n)$ with a fixed function $B : \mathbb{R} \rightarrow \mathbb{R}^{s \times s}$. In order to obtain sufficiently high orders at the boundary steps, more general matrices A_0, A_N are required, but $K_0 = K_N = K$ and $B_N = B(\sigma_N)$ in the end step are also used in this paper. Since our focus now is more on the practical implementation of the Peer triplets, we re-designed the boundary steps from [19]. The increased effort for boundary steps not in diagonally-implicit form is a minor fraction of the overall effort in the solution of the full boundary value problem only. However, we admit that the memory requirement is multiplied there and this may lead to difficulties for large problems. Hence we have re-designed the boundary steps and will provide fast iteration methods with triangular coefficients \tilde{A}_0, \tilde{A}_N , requiring again the solution of systems with m unknowns only. This was indeed possible with positive definite diagonal $K_n \equiv K \succ 0$ for all n .

All in all, a Peer triplet now consists of a set of 5 coefficient matrices,

$$A_0, A, A_N, K \succ 0, \text{ and } B(\sigma_n), n = 1, \dots, N.$$

The additional matrices \tilde{A}_0, \tilde{A}_N are not part of the triplet as integration method but a supplement simplifying the solution in the boundary steps. For a shorter notation, we will use the same symbol for a coefficient matrix like A and its Kronecker product $A \otimes I_m$ as a mapping from the space R^{sm} to itself. We also stick to A_n in general to avoid doubling of equations.

3 First order optimality conditions

The first-order optimality conditions for the optimal control problem (1)–(3) with some Lagrange multiplier $p(t) \in \mathbb{R}^m$ read [9, 24]

$$y'(t) = f(y(t), u(t)), \quad t \in (0, T], \quad y(0) = y_0, \quad (6)$$

$$p'(t) = -\nabla_y f(y(t), u(t))^T p(t), \quad t \in [0, T], \quad p(T) = \nabla_y \mathcal{C}(y(T))^T, \quad (7)$$

$$-\nabla_u f(y(t), u(t))^T p(t) \in N_U(u(t)), \quad t \in [0, T], \quad (8)$$

with the normal cone mapping

$$N_U(u) = \{w \in \mathbb{R}^d : w^T(v - u) \leq 0 \text{ for all } v \in U_{ad}\}.$$

We recall a few facts from [9]. Under appropriate regularity conditions, there exists a local solution (y^*, u^*, p^*) such that the first-order optimality conditions (6)–(8) are necessarily satisfied. These conditions are also sufficient, if the Hamiltonian $H(y, u, p) := p^T f(y, u)$ satisfies a coercivity assumption. Then, the control uniqueness property yields the existence of a locally unique minimizer $u = u(\hat{y}, \hat{p})$ of the Hamiltonian over all $u \in U_{ad}$, if (\hat{y}, \hat{p}) is sufficiently close to (y^*, p^*) .

Applying a two-step Peer triplet to (1)–(3), we get the discrete constraint nonlinear optimal control problem

$$\begin{aligned} & \text{minimize } \mathcal{C}(y_h(T)) \\ & \text{subject to } A_0 Y_0 = a \otimes y_0 + h_0 K F(Y_0, U_0), \end{aligned} \quad (9)$$

$$A_n Y_n = B_n Y_{n-1} + h_n K F(Y_n, U_n), \quad n = 1, \dots, N, \quad (10)$$

with an approximation $y_h(T) = (w^T \otimes I_m) Y_N \approx y(T)$, $w \in \mathbb{R}^s$, at the final time point. Since $K = (\kappa_{ii})_{i=1}^s$ is a positive definite diagonal matrix, the first order optimality conditions now read [19]

$$A_0 Y_0 = a \otimes y_0 + h_0 K F(Y_0, U_0), \quad (11)$$

$$A_n Y_n = B_n Y_{n-1} + h_n K F(Y_n, U_n), \quad n = 1, \dots, N, \quad (12)$$

$$A_N^T P_N = w \otimes p_h(T) + h_N K \nabla_Y F(Y_N, U_N)^T P_N, \quad (13)$$

$$A_n^T P_n = B_{n+1}^T P_{n+1} + h_n K \nabla_Y F(Y_n, U_n)^T P_n, \quad 0 \leq n \leq N-1, \quad (14)$$

$$-h_n \kappa_{ii} \nabla_u f(Y_{ni}, U_{ni})^T P_{ni} \in N_U(U_{ni}), \quad 0 \leq n \leq N, \quad i = 1, \dots, s. \quad (15)$$

Here, $p_h(T) = \nabla_y \mathcal{C}(y_h(T))^T$ and the Jacobians of F are block diagonal matrices $\nabla_Y F(Y_n, U_n) = \text{blockdiag}_i(\nabla_y f(Y_{ni}, U_{ni}))$. Since $h_n \kappa_{ii} > 0$, (15) can be simplified to $-\nabla_u f(Y_{ni}, U_{ni})^T P_{ni} \in N_U(U_{ni})$. Hence, the control uniqueness property mentioned above guarantees the existence of a local minimizer U_{ni} of the Hamiltonian $H(Y_{ni}, U, P_{ni})$ over all $U \in U_{ad}$, which shows the importance of having $\kappa_{ii} > 0$ for all diagonal entries of K . Such positivity conditions also arise in the context of classical Runge-Kutta methods or W-methods, see [9, Theorem 2.1] and [20, Chapter 5.2].

4 Gradient-based optimization

The cost function $\mathcal{C}(y_h(T))$ can be associated with the vector of control values

$$U = (U_{01}^\top, \dots, U_{0s}^\top, U_{11}^\top, \dots, U_{Ns}^\top)^\top \in \mathbb{R}^{sd(N+1)}$$

by interpreting $y_h(T)$ as function of U and defining $\mathcal{C}(U) := \mathcal{C}(y_h(U))$. The whole gradient of $\mathcal{C}(U)$ can then be computed from

$$\nabla_{U_{ni}} \mathcal{C}(U) = h_n \kappa_{ii} \nabla_u f(Y_{ni}, U_{ni})^\top P_{ni}, \quad 0 \leq n \leq N, i = 1, \dots, s,$$

following, e.g., the approach from [10]. Such approximate gradients can be used to set up an iterative procedure to approximate the control vector starting from an initial guess $U^{(0)}$. Increments $\Delta U^{(k)}$ to get updates from

$$U^{(k+1)} := U^{(k)} + \Delta U^{(k)}, \quad k = 0, 1, \dots \quad (16)$$

can be efficiently computed by gradient-based optimization algorithms such as *interior-point* [6], *sequential-quadratic-programming* [23], and *trust-region-reflective* [7] for large-scale sparse problems with continuous objective function and first derivatives. Various implementations are available in commercial software packages like Matlab, Mathematica, and others.

Given $U^{(k)}$, approximations for (Y_n, P_n) are computable by a forward-backward marching scheme. Since the discrete state equations (11)–(12) do not depend on the multipliers P_n , all Y_n for $n = 0, \dots, N$, are computable from a simple forward calculation. Then, using the updated values Y_n , one computes $p_h(T) = \nabla_y \mathcal{C}(y_h(T))^\top$ with $y_h(T) = (w^\top \otimes I)Y_N$ before marching the steps (13)–(14) backwards for $n = N, \dots, 0$, solving the discrete costate equations for all P_n .

Since the optimal control $u(t)$ minimizes the Hamiltonian $H(y, u, p) = p^\top f(y, u)$, we may compute an improved approximation of the control by the following minimum principle:

$$U_{ni}^\ddagger = \arg \min_{U \in U_{ad}} H(Y_{ni}, U, P_{ni}), \quad 0 \leq n \leq N, i = 1, \dots, s, \quad (17)$$

if Y_{ni} or P_{ni} are approximations of higher-order. Often, a higher convergence order for P_{ni} can be observed in practice, leading to a better approximation for U_{ni}^\ddagger compared to U_{ni} .

5 Properties of Peer triplets

Here, we shortly review those results from our previous paper [19] that are necessary for the redesign of the boundary methods. We now consider only methods with the same order $q < s$ for the original scheme and its adjoint.

5.1 The standard method

As for multi-step methods, order conditions are derived by Taylor expansion of the residuals if exact solution values are used as arguments of the numerical scheme. For variable stepsizes, these conditions depend on the stepsize ratio $\sigma_n = h_n/h_{n-1}$ in the scaling matrix $S_{n,q} = \text{diag}_i(\sigma_n^{i-1}) \in \mathbb{R}^{q \times q}$. Compact formulations of the order conditions are possible with the vector of node powers $\mathbf{c}^k = (c_1^k, \dots, c_s^k)^\top$, the Vandermonde matrix $V_q = (\mathbf{1}, \mathbf{c}, \dots, \mathbf{c}^{q-1}) \in \mathbb{R}^{s \times q}$, the Pascal matrix

$\mathcal{P}_q = \left(\begin{smallmatrix} (j-1) \\ i-1 \end{smallmatrix} \right) \in \mathbb{R}^{q \times q}$, and the scaled shift matrix $\tilde{E}_1 = (i\delta_{i+1,j}) \in \mathbb{R}^{q \times q}$ which commutes with $\mathcal{P}_q = \exp(\tilde{E}_q)$. Both the standard forward step (12) and its adjoint (14) posses local order q if

$$A_n V_q - KV_q \tilde{E}_q = B_n V_q \mathcal{P}_q^{-1} S_{n,q}^{-1} \equiv B(1) V_q \mathcal{P}_q^{-1}, \quad (18)$$

$$A_n^\top V_q + KV_q \tilde{E}_q = B_{n+1}^\top V_q S_{n+1,q} \mathcal{P}_q \equiv B(1)^\top V_q \mathcal{P}_q. \quad (19)$$

Since the matrices on the left-hand sides of both equations are independent of σ_n, σ_{n+1} by design, the same holds for the other terms which is highlighted by the right-most expressions. Combining both conditions with varying parameter σ leads to a very restricted form of the following matrix playing a central role [19, Lemma 3.1],

$$\mathcal{Q}_{q,q}(\sigma) = e_1 e_1^\top \in \mathbb{R}^{q \times q}, \quad \text{where } \mathcal{Q}_{q,r}(\sigma) := V_q^\top B(\sigma) V_r \mathcal{P}_r^{-1}, \quad q, r \leq s. \quad (20)$$

This property is also the reason why the uniform local order should be smaller than s , since for $q = r = s$ no freedom is left for fulfilling σ -dependent conditions. As a consequence it turned out that the following congruent $s \times s$ - matrices

$$\hat{A}_n = V_s^\top A_n V_s, \quad \hat{K} := V_s^\top K V_s, \quad \hat{B}(\sigma) := V_s^\top B(\sigma) V_s \quad (21)$$

also possess very restricted forms with few free parameters. Since we are mainly interested here in four-stage methods, we depict this form for the standard method with order $q = 3 = s - 1$:

$$\hat{A} = \begin{pmatrix} 1 & 1 & 1 & 1 \\ 0 & \frac{1}{2} & \frac{2}{3} & \hat{a}_{24} \\ 0 & \frac{1}{3} & \frac{2}{4} & \hat{a}_{34} \\ \hat{a}_{41} & \hat{a}_{42} & \hat{a}_{43} & \hat{a}_{44} \end{pmatrix}, \quad \hat{B}(\sigma) = \begin{pmatrix} 1 & 1 & 1 & 1 \\ 0 & 0 & 0 & \hat{b}_{24}(\sigma) \\ 0 & 0 & 0 & \hat{b}_{34}(\sigma) \\ \hat{a}_{41} & \hat{b}_{42}(\sigma) & \hat{b}_{43}(\sigma) & \hat{b}_{44}(\sigma) \end{pmatrix}, \quad (22)$$

and $\hat{K} = \text{hankel}(1, \frac{1}{2}, \frac{1}{3}, \frac{1}{4}, \hat{k}_5, \hat{k}_6, \hat{k}_7)$ is a Hankel matrix coinciding with the Hilbert matrix in its first 4 antidiagonals. The first row and column of $\hat{B}(\sigma)$ coincide with that of \hat{A} due to the conditions (18), (19) of lowest order, and with the exception of $\hat{b}_{44}(\sigma)$ its other elements are fixed by the order $q = 3$. Since both methods in this paper will also satisfy (35) below, we have already fixed $\hat{a}_{14} = 1$. A drawback of the sparing parametrization through (21), (22) is that the triangular form of A itself is lost and has to be enforced by an appropriate set of equations. As a consequence the only free parameters of the standard Peer method will be \hat{a}_{41} and $\hat{b}_{44}(\sigma)$ in (22) and the nodes c_i , of course.

A critical requirement for the standard method is zero stability which may be very demanding for variable stepsizes. For the trivial ODE $y' = 0$, the stability matrix of the forward step (12), $Y_n = A^{-1} B_n Y_{n-1}$, of the standard method is $\bar{B}_n := A^{-1} B_n$ and for the adjoint step (14) it is $A^{-\top} B_{n+1}^\top = A^{-\top} \bar{B}_{n+1}^\top A^\top$. Zero stability requires that arbitrarily long products, e.g., $\bar{B}_n \cdots \bar{B}_{k+1}$, $n > k$, are uniformly bounded. Since $\hat{A}^{-1} \hat{B}(\sigma) = V_s^{-1} \bar{B}(\sigma) V_s$ is similar to the stability matrix $\bar{B}(\sigma)$, based on the representation (22) in [19], the construction of a σ -independent weight matrix $W \in \mathbb{R}^{s \times s}$ was incorporated into the design of all standard methods, which block-diagonalizes all matrices simultaneously,

$$W^{-1} \bar{B}(\sigma) W = \begin{pmatrix} 1 & 0 \\ 0 & B_{se}(\sigma) \end{pmatrix}, \quad \text{such that } \|B_{se}(\sigma)\|_\infty \leq \tilde{\gamma} < 1 \quad (23)$$

for σ near one. In particular, (23) states that 1 is an eigenvalue of $\bar{B}(\sigma)$. This follows from the order conditions (18), (19), from which the exact form of the corresponding eigenvectors can be deduced as

$$\bar{B}(\sigma)\mathbb{1} = A^{-1}B(\sigma)\mathbb{1} = \mathbb{1}, \quad (\mathbb{1}^\top A)\bar{B}(\sigma) = (\mathbb{1}^\top A). \quad (24)$$

The weighted norm corresponding to (23) satisfies

$$\|\bar{B}(\sigma)\| := \|W^{-1}\bar{B}(\sigma)W\|_\infty = 1, \quad \sigma \in [\underline{\sigma}, \bar{\sigma}], \quad 0 < \underline{\sigma} < 1 < \bar{\sigma}, \quad (25)$$

where a large interval $[\underline{\sigma}, \bar{\sigma}]$ was one of the design objectives. Based on this property, convergence of the global error with order $q-1=2$ was proven rigorously in [19, Theorem 6.1].

In order the regain global order $q=3$, an additional super-convergence property is employed, which prohibits the propagation of the leading term of the local error. Denoting evaluations of the exact solution by boldface as in $\mathbf{y}_n = (y^*(t_{ni}))_{i=1}^n$, $\mathbf{y}'_n = ((y^*)'(t_{ni}))_{i=1}^n$, etc., the local errors of the standard method are defined by

$$\tau_n^Y = \mathbf{y}_n - A_n^{-1}(B_n \mathbf{y}_{n-1} + h_n K \mathbf{y}'_n), \quad n = 1, \dots, N, \quad (26)$$

$$\tau_n^P := \mathbf{p}_n - A_n^{-\top}(B_{n+1}^\top \mathbf{p}_{n+1} - h_n K \mathbf{p}'_n), \quad n = 0, \dots, N-1, \quad (27)$$

and the order conditions (18), (19) lead to the following expressions of these errors [19]:

$$\tau_n^Y = h_n^q \beta_{q,n}(\sigma_n) y^{*(q)}(t_n) + O\left(h_n^{q+1} \|y^{*(q+1)}\|_{[n]}\right), \quad (28)$$

$$\beta_{q,n}(\sigma) := \frac{1}{q!} A_n^{-1} (A_n \mathbf{c}^q - B_n (\mathbf{c} - \mathbb{1})^q \sigma^{-q} - q K \mathbf{c}^{q-1}), \quad n \geq 1, \quad (29)$$

$$\tau_n^P = h_n^q \beta_{q,n}^\dagger(\sigma_{n+1}) p^{*(q)}(t_n) + O\left(h_n^{q+1} \|p^{*(q+1)}\|_{[n]}\right), \quad (30)$$

$$\beta_{q,n}^\dagger(\sigma) = \frac{1}{q!} A_n^{-\top} (A_n^\top \mathbf{c}^q - B_{n+1}^\top (\mathbb{1} + \sigma \mathbf{c})^q + q K^\top \mathbf{c}^{q-1}), \quad n < N. \quad (31)$$

As the theoretical basis of stepsize control, we emphasize here the localized dependence on derivatives and write the interval $[0, T] = \bigcup_{n=0}^N \pi_n$ as the union of the subintervals $\pi_n := [t_n, t_{n+1}]$. To take into account the two-step form of the Peer methods, for $\phi \in C[0, T]$, we use the definition

$$\|\phi\|_{[n]} := \max\{\|\phi(t)\| : t \in \pi_{n-1} \cup \pi_n \cup \pi_{n+1}\}, \quad 0 \leq n \leq N, \quad (32)$$

where $\pi_{-1} = \pi_{N+1} = \emptyset$. Through the iterated recursion (12), the local error τ_k^Y is multiplied by long products $\bar{B}_n \cdots \bar{B}_{k+1} \tau_k^Y$ which by (23), (24) converge as

$$\bar{B}_n \cdots \bar{B}_{k+1} = \mathbb{1} \mathbb{1}^\top A + O(\tilde{\gamma}^{n-k}), \quad n - k \rightarrow \infty,$$

see (23), with an analogous version for the adjoint matrices $A^\top B_{n+1}$. Hence, there is no accumulation of leading error terms of the standard method under the super-convergence conditions

$$\mathbb{1}^\top A \beta_q(\sigma) = 0, \quad \mathbb{1}^\top A^\top \beta_q^\dagger(\sigma) = 0, \quad (33)$$

and the global order $q = s-1 = 3$ is regained, see [19, Lemma 6.1]. By purpose, we did not specify here the range for the stepsize ratio σ . In fact, if (33) is satisfied for arbitrary $\sigma \in \mathbb{R}$, the standard Peer method (as in `AP4o33vgi` below) will converge for *general grids* satisfying only the restriction

in (25). On the other hand, if (33) is satisfied for $\sigma = 1$ only, order $q = s - 1 = 3$ still holds for *smooth grids* satisfying

$$|\sigma_n - 1| \leq \eta h_n, \quad n = 0, \dots, N, \quad (34)$$

with some moderately large constant η (e.g. $\eta = 15$). The other triplet **AP4o33vsi** below belongs to this class. As a trade-off for its inferior convergence properties, it possesses a much larger angle of $A(\alpha)$ -stability than **AP4o33vgi**.

In the design process in [19] it turned out that a special feature of the standard method leads to improved properties concerning accuracy and stability. In addition to the order conditions (18), (19) with $q = s - 1$, these methods satisfy

$$e_1^\top \hat{A} = \mathbb{1}^\top, \quad c_s = 1. \quad (35)$$

An essential consequence is that $\mathbb{1}^\top A = e_s^\top$ holds, leading to the simple left eigenvector $e_s^\top \bar{B}(\sigma) = e_s^\top$ of the stability matrix. Hence, the last stage of the Peer method may also be written as

$$Y_{ns} = Y_{n-1,s} + h_n \sum_{j=1}^s \kappa_{jj} f(Y_{nj}, U_{nj}), \quad (36)$$

which, together with $c_s = 1$, resembles a final stage of a Runge-Kutta method since $Y_{n-1,s} \cong y(t_n)$. We say that such methods have LSRK form (*Last Stage is Runge-Kutta*). However, we stress the fact that this last Runge-Kutta step is not prone to order reduction since the stage increments $f(Y_{nj}, U_{nj})$ have full stage order q due to the two-step structure of the Peer method.

5.2 Boundary methods

Exceptional coefficients A_0, A_N in general form are required for the boundary steps since with triangular matrices the first starting stage in (11) and the first backward stage (with index s) of the adjoint end condition (13) would be implicit Euler steps with insufficient local order two. Since the boundary steps are applied only once each, their required local order is identical with the global order q . For the starting step, the forward order condition reads [19]

$$A_0 V_q = a e_1^\top + K V_q \tilde{E}_q. \quad (37)$$

Since $\tilde{E}_q e_1 = 0$, we deduce that $a = A_0 \mathbb{1}$. The adjoint order condition (19) for the starting step may be compared to the one of the standard method, yielding

$$A_0^\top V_q = B(\sigma_1)^\top V_q S_q(\sigma_1) \mathcal{P}_q - K V_q \tilde{E}_q = A^\top V_q.$$

According to (19), here all 4 product terms are σ -independent, showing that $V_q^\top (A_0 - A) = 0$. Hence, for $q = s - 1$, the matrix A_0 is a rank-1-modification of A itself,

$$A_0 = A + V_s^{-\top} e_s \phi_0^\top, \quad \phi_0 \in \mathbb{R}^s,$$

since the last row of V_s^{-1} is orthogonal to all columns of V_q , $q < s$. The coefficient a now is $a = A \mathbb{1} + (e_1^\top \phi_0) V_s^{-\top} e_s$ and with respect to (18), condition (37) may be rewritten as

$$(A \mathbb{1} + (e_1^\top \phi_0) V_s^{-\top} e_s) e_1^\top - V_s^{-\top} e_s \phi_0^\top = A V_q - K V \tilde{E}_q = B(\sigma_1) V_q \mathcal{P}_q^{-1} S_q(\sigma_1) \equiv B(1) V_q \mathcal{P}_q^{-1}.$$

Multiplying by V_s^\top from the left and recalling that $V_s^\top A \mathbb{1} = \hat{A}e_1$ gives

$$\hat{A}e_1 e_1^\top + e_s((e_1^\top \phi_0)e_1 - \phi_0)^\top = V_s^\top B(1)V_q \mathcal{P}_q^{-1} = \mathcal{Q}_{s,q}(1), \quad (38)$$

with the matrix \mathcal{Q} from (20). Since $\mathcal{Q}_{s,q}e_1 = \hat{B}e_1 = \hat{A}e_1$, the first column in (38) is satisfied for arbitrary ϕ_0 and the same holds for the first q rows, since $\mathcal{Q}_{q,q} = e_1 e_1^\top$ by (20). The remaining entries yield $e_j^\top \phi_0 = -e_s^\top \mathcal{Q}_{s,q} e_j$, $j = 2, \dots, q$.

In an analogous way, the forward condition for the end step (12) means that

$$A_N V_q = B_N V_q \mathcal{P}_q^{-1} S_{N,q}^{-1} - K V_q \tilde{E}_q = A V_q,$$

leading to $(A_N - A)V_q = 0$, and for $q = s - 1$ to

$$A_N = A + \phi_N e_s^\top V_s^{-1}$$

with parameter $\phi_N \in \mathbb{R}^s$. The order condition for the adjoint starting step (13) is [19]

$$A_N^\top V_q + K V_q \tilde{E}_q = w \mathbb{1}_q^\top, \quad (39)$$

revealing that $w = A_N^\top V_s e_1 = A_N^\top \mathbb{1} = A^\top \mathbb{1} + V_s^{-\top} e_s \phi_N^\top \mathbb{1}$. Multiplying (39) by V_s^\top from the left and reminding (19), we obtain

$$\begin{aligned} V_s^\top w \mathbb{1}_q^\top &= V_s^\top (A^\top \mathbb{1} + V_s^{-\top} e_s \phi_N^\top \mathbb{1}) \mathbb{1}_q^\top = \\ &= \hat{A}^\top e_1 \mathbb{1}_q^\top + (\phi_N^\top \mathbb{1}) e_s \mathbb{1}_q^\top \stackrel{(39)}{=} V_s^\top (A^\top V_q + K V_q \tilde{E}_q) + e_s \phi_N^\top V_q = V_s^\top B(1)^\top V_q \mathcal{P}_q + e_s \phi_N^\top V_q. \end{aligned} \quad (40)$$

Multiplying by \mathcal{P}_q^{-1} from the right and reminding $\mathbb{1}^\top \mathcal{P}_q^{-1} = e_1^\top$, the first $q = s - 1$ rows of the lower equation have the form $\mathbb{1} e_1^\top \in \mathbb{R}^{q \times q}$ on both sides by (22). And the first entry of row number s is satisfied for arbitrary ϕ_N , but the remaining entries lead to $q - 1$ restrictions. We collect these results now.

Lemma 5.1 *For $q = s - 1$ let A_0 satisfy the order conditions (37), (19) for $n = 0$ and A_N the conditions (39), (18) for $n = N$ and let (20) hold. Then, with $\phi_0, \phi_N \in \mathbb{R}^s$ it holds*

$$A_0 = A + V_s^{-\top} \phi_0, \quad A_N = A + \phi_N e_s^\top V_s^{-1}, \quad (41)$$

where

$$e_j^\top \phi_0 = -e_s^\top \mathcal{Q}_{s,q}(1) e_j, \quad \phi_N^\top V_q \mathcal{P}_q^{-1} e_j = -\hat{b}_{js}(1), \quad j = 2, \dots, q. \quad (42)$$

The Lemma shows that in the boundary methods there are only 2 free parameters in the rank-one representation (41) of A_0, A_N , each.

Remark 5.1 *The fact that the conditions for ϕ_0, ϕ_N can be fulfilled although the left hand sides of (38) and (40) have rank 2 only while the matrix $B(1)$ on the right hand side may be a full matrix, in principle, may seem like a lucky coincidence. However, the analysis in [18] revealed the strong relation between the coefficients of the standard and the boundary methods forced by the many order conditions. The design of the standard methods has taken account for these side conditions.*

Finally, we have to complement the definition of the local errors (28), (30) for the exceptional order conditions (37), (39) at the boundaries through

$$\beta_{q,0} = \frac{1}{q!} (\mathbf{c}^q - q A_0^{-1} K \mathbf{c}^{q-1}), \quad \beta_{q,N}^\dagger = \frac{1}{q!} (\mathbf{c}^q + q A_N^{-1} K \mathbf{c}^{q-1} - \mathbb{1}). \quad (43)$$

These coefficients do not depend on σ .

5.3 Triangular iterations at the boundaries

Although the two boundary steps require a fraction of the overall computational effort only, with full matrices A_0, A_N the memory requirement for nonlinear systems of size $(sm) \times (sm)$ may be prohibitive for large-scale problems. This difficulty may be eliminated by reviving an idea from our paper [15] employing iterations with triangular approximations \tilde{A}_0, \tilde{A}_N of the matrices A_0, A_N . Implementation of this iteration requires only minor changes to the standard step if the subdiagonals of \tilde{A}_0 and A_0 as well as of \tilde{A}_N and A_N coincide, which means that

$$R_0 := A_0 - \tilde{A}_0, \quad R_N := A_N - \tilde{A}_N \quad (44)$$

are upper triangular. In this case, the boundary steps can be solved stage by stage and approximations for previous stages can be overwritten immediately, avoiding additional memory requirements. We shortly describe this property for an approximate Newton step of the starting method (11). Here,

$$(\tilde{A}_0 - h_0 K \mathbf{J}_0)(Y_0^{(k+1)} - Y_0^{(k)}) = a \otimes y_0 + h_0 K F(Y_0^{(k)}, U_0) - A_0 Y_0^{(k)}, \quad k \geq 0, \quad (45)$$

with the Jacobian $\mathbf{J}_0 = \text{blockdiag}_i(J_{0i})$, $J_{0i} = \nabla_y f(y_0, e_1^\top V_4^{-1} U_0)$, $i = 1, \dots, s$. Since $\tilde{A}_0 = (\tilde{a}_{ij}^{(0)})$ is lower triangular, the equation for $Y_{0i}^{(k+1)}$, $i = 1, \dots, s$, may be solved successively as

$$\begin{aligned} & (\tilde{a}_{ii}^{(0)} I - h_0 \kappa_{ii} J_{0i})(Y_{0i}^{(k+1)} - Y_{0i}^{(k)}) \\ &= - \sum_{j=1}^{i-1} \tilde{a}_{ij}^{(0)} (Y_{0j}^{(k+1)} - Y_{0j}^{(k)}) + a_i y_0 + h_0 \kappa_{ii} f(Y_{0i}, U_{0i}) - \sum_{j=1}^s a_{ij}^{(0)} Y_{0j}^{(k)} \\ &= a_i y_0 + h_0 \kappa_{ii} f(Y_{0i}, U_{0i}) - \sum_{j=1}^{i-1} \tilde{a}_{ij}^{(0)} Y_{0j}^{(k+1)} - \sum_{j=i}^s (r_{ij}^{(0)} + \delta_{ij} \tilde{a}_{ii}^{(0)}) Y_{0j}^{(k)}. \end{aligned}$$

Obviously, the old value $Y_{0i}^{(k)}$ may be overwritten by $Y_{0i}^{(k+1)}$ after solving stage equation number i .

For linear autonomous problems, the error of the iteration for the end equations obeys the recursion $\check{Y}_n^{(k+1)} = (\tilde{A}_n - h_n K \otimes J_n)^{-1} (\tilde{A}_n - A_n) \check{Y}_n^{(k)}$, $n \in \{0, N\}$. Considering an eigenvalue λ of J_n and $z = h_n \lambda$, the linear convergence of the iteration is described by the matrix

$$\mathcal{S}_n(z) := (\tilde{A}_n - z K)^{-1} (\tilde{A}_n - A_n), \quad z \in \mathbb{C}. \quad (46)$$

For the two Peer triplets discussed below, new boundary methods have been constructed by minimizing the spectral radius $\rho_{\mathbb{R}}$ of the iteration matrix (46) along the negative real axis, resulting in small contraction factors below 0.1. Also the spectral radius ρ_{α} in the sector of $A(\alpha)$ -stability will be reported, since this sector is the largest one where an application of the triplet may be advised. Since these contractions factors are quite small, they might scarcely slow down the convergence of the Newton iteration.

These contraction factors are also valid for the adjoint iterations. The iteration matrix for (14), for instance, is

$$\mathcal{S}_0^\dagger(z) = (\tilde{A}_0^\top - z K)^{-1} (\tilde{A}_0 - A)^\top$$

and possesses the same eigenvalues as $\mathcal{S}_0(z)$ since eigenvalues are invariant if two matrix factors are commuted.

6 Two modified Peer triplets

Here we present modifications of two Peer triplets from [19] with definite matrices $K \succ 0$. In order to avoid ambiguities, the letter **i** (for iteration in the boundary methods) is added to their old names. Beyond the order of convergence, important properties of the triplets are $A(\alpha)$ -stability and zero-stability (25), the leading error constants

$$err_{q,n} = \|\beta_{q,n}(1)\|_\infty, \quad err_{q,n}^\dagger = \|\beta_{q,n}^\dagger(1)\|_\infty,$$

and the precise form of the super-convergence condition (52). Also, the Jacobians $A_n - h_n K \mathbf{J}_n = K(K^{-1}A_n - h_n \mathbf{J}_n)$ of the original boundary steps should be well-conditioned for stiff problems with eigenvalues of \mathbf{J}_n in the left complex half-plane, and we require the eigenvalue conditions

$$\mu_n := \min_j \operatorname{Re} \lambda_j(K^{-1}A_n) > 0, \quad n \in \{0, N\}. \quad (47)$$

6.1 The 'pulcherrima' triplet AP4o33vgi

For the triplet **AP4o33vgi** (Adjoint Peer method with 4 stages, orders $q = 3$ for state and adjoint, variable stepsizes, general grids, iteration), the standard method is given with the nodes and coefficients

$$\mathbf{c}^\top = \left(0, \frac{1}{3}, \frac{2}{3}, 1\right), \quad K = \operatorname{diag}\left(\frac{1}{8}, \frac{3}{8}, \frac{3}{8}, \frac{1}{8}\right) \succ 0, \quad A = \begin{pmatrix} 1 & \cdot & \cdot & \cdot \\ -\frac{9}{4} & \frac{9}{4} & \cdot & \cdot \\ \frac{9}{4} & -\frac{9}{2} & \frac{9}{4} & \cdot \\ -1 & \frac{9}{4} & -\frac{9}{4} & 1 \end{pmatrix}. \quad (48)$$

Vanishing entries are replaced by dots in order to highlight the structure. The nodes and the diagonals of K belong to the pulcherrima quadrature rule having positive weights. Since $c_4 = 1$ and $\mathbf{1}^\top A = e_s^\top$, it has LSRK form. A further remarkable property is that the standard method is its own adjoint, which means that if the grid on the interval $[0, T]$ is flipped at its midpoint, the original scheme is reproduced. Since this property is of interest, we require it for the whole triplet. Algebraically, it may be described with the flip permutation $\Pi := (\delta_{i,s+1-i}) \in \mathbb{R}^{s \times s}$. The nodes are symmetric, $\Pi \mathbf{c} = \mathbf{1} - \mathbf{c}$ and the coefficients satisfy

$$\Pi A \Pi = A^\top, \quad \Pi K \Pi = K, \quad \Pi B(\sigma) \Pi = B(\sigma^{-1})^\top, \quad w = \Pi a, \quad \Pi A_N \Pi = A_0^\top. \quad (49)$$

The condition for $B(\sigma)$ is more general than in [19], where it was used for $\sigma = 1$ only and is based on the fact that by a flip of the grid stepsize ratios are inverted. Hence, the triplet **AP4o33vgi** also has a slight modification in the last element of the third coefficient of the standard method

$$\hat{b}_{44}(\sigma) = \frac{1}{804} \left(132\sigma + \frac{65}{\sigma} - 149 \right), \quad (50)$$

$$\hat{B}(\sigma) = \begin{pmatrix} 1 & 1 & 1 & 1 \\ \cdot & \cdot & \cdot & \frac{1}{36\sigma} \\ \cdot & \cdot & \cdot & \cdot \\ 0 & \frac{\sigma}{36} & \frac{\sigma}{18} & \hat{b}_{44}(\sigma) \end{pmatrix}, \quad W = \begin{pmatrix} 1 & -2 & \frac{24}{5} & -\frac{9}{2} \\ 1 & -\frac{4}{3} & 0 & \frac{3}{2} \\ 1 & -\frac{2}{3} & -\frac{8}{5} & \frac{3}{2} \\ 1 & 0 & 0 & 0 \end{pmatrix}. \quad (51)$$

triplet	s, q	nodes	α	$\sigma \in$	err_3	err_3^\dagger
AP4o33vgi	4, 3	[0, 1]	61.59°	[0.57, 2.10]	9.8e-3	9.8e-3
AP4o33vsi	4, 3	(0, 1]	83.74°	[0.65, 1.80]	5.1e-2	3.2e-2

Table 1: Properties of the standard methods.

triplet	Starting method					End method				
	$\rho_{\mathbb{R},0}$	$\rho_{\alpha,0}$	μ_0	$err_{3,0}$	$err_{3,0}^\dagger$	$\rho_{\mathbb{R},N}$	$\rho_{\alpha,N}$	μ_N	$err_{3,N}$	$err_{3,N}^\dagger$
AP4o33vgi	6.4e-2	0.155	4.31	5.2e-3	9.5e-3	6.4e-2	0.155	4.31	9.5e-3	5.2e-3
AP4o33vsi	3.4e-2	0.126	5.65	5.2e-3	2.1e-2	6.6e-2	0.217	2.55	6.7e-2	4.1e-2

Table 2: Properties of the boundary methods.

The new coefficient also leads to a slightly larger interval $[\underline{\sigma}, \bar{\sigma}] = [0.57, 2.1]$ of uniform zero-stability (25) and equation (51) contains a better conditioned version of the corresponding weight matrix W . The stability region $\{z \in \mathbb{C} : \varrho(M(z)) \leq 1\}$, $M(z) := (A - zK)^{-1}B$, has a simple form. Its complement is kidney-shaped, contained in $[-4, 31] \times [-22, 22]$, and touches the imaginary axis at $z = 0$ due to consistency. The method is $A(\alpha)$ -stable with $\alpha = 61.59^\circ$. A remarkable property is that it even satisfies $\varrho(M(i\xi)) \leq 1$ for $\xi \in [-1, 1]$.

Since $c_1 = 0$ and $Ae_1 = e_1$, this triplet possesses LSRK form also for the adjoint equation, but this is also clear from the flip condition (49). Important consequences of the LSRK property are that super-convergence occurs for arbitrary stepsize ratios σ :

$$\mathbb{1}^\top A\beta_3(\sigma) = e_4^\top \beta_3(\sigma) \equiv 0, \quad \mathbb{1}^\top A^\top \beta_3^\dagger(\sigma) = e_1^\top \beta_3^\dagger(\sigma) \equiv 0, \quad \sigma \in \mathbb{R}, \quad (52)$$

for the leading error coefficients (29), (31). Essential properties of the standard method, the stage number and order, range of nodes, stability angle α , interval of uniform zero stability and error constants, are collected in Table 1.

The boundary methods are re-designed now in order to obtain fast iterations (45) with triangular approximations \tilde{A}_0, \tilde{A}_N . Not only the free diagonal parameters of these matrices will be used, but also the two free parameters of A_0 resp. A_N itself. For the rank-one-representations (41), the flip condition (49) means that

$$\Pi A_N \Pi = \Pi A \Pi + \Pi \phi_N e_s^\top V_s^{-1} \Pi \stackrel{!}{=} A_0^\top = A^\top + \phi_0 e_s^\top V_s^{-1} \Pi \Rightarrow \phi_0 = \Pi \phi_N,$$

and for the starting method, we simply use $\tilde{A}_0 = \Pi \tilde{A}_N \Pi$. As mentioned before, for the triangular iteration, we consider the contraction factors

$$\rho_{\mathbb{R},n} := \max\{\varrho(S_n(z)) : z \in (-\infty, 0)\}, \quad \rho_{\alpha,n} := \max\{\varrho(S_n(z)) : |\arg(z) - \pi| \leq \alpha\}, \quad (53)$$

where $\varrho(\cdot)$ means the spectral radius and α is the angle of $A(\alpha)$ -stability of the method listed in Table 1. In fact, only the contraction factor $\rho_{\mathbb{R},N}$ on the negative real axis was minimized but the factor $\rho_{\alpha,N}$ still is acceptable. The matrices for AP4o33vgi are printed in Appendix A1 and the contraction factors are $\rho_{\mathbb{R},0} = \rho_{\mathbb{R},N} = 0.0637$, $\rho_{\alpha,0} = \rho_{\mathbb{R},N} = 0.155$, see also Table 2.

Since $c_s = 1$, the best approximation of order s at the end point would be obtained with $w^\top = e_s^\top = \mathbb{1}^\top V_s^{-1}$ by $y_h(T) = e_s^\top Y_N = Y_{Ns}$. However, (39) requires that $w^\top = \mathbb{1}^\top A_N$ or

$$w^\top V_s = \mathbb{1}^\top \hat{A}_N V_s \stackrel{(41)}{=} e_1 \hat{A} + \mathbb{1}^\top \phi_N e_s^\top = (1, \dots, 1, 1 + \mathbb{1}^\top \phi_N).$$

This means that $w^T Y_N = e_s^T Y_N + (\mathbb{1}^T \phi_N) e_s^T V_s^{-1} Y_N = Y_{Ns} + O(h_N^{s-1})$ is an $O(h_N^q)$ perturbation of the 'best' approximation with the order q of the triplet and the choice $w = e_s$ would give away one useful degree of freedom in the end method.

6.2 The triplet AP4o33vsi for smooth grids

Although the pulcherrima triplet has many favourable properties, its stability angle below 62° may be too small for some applications. By sacrificing some of these properties, a Peer triplet with much larger angle could be designed in [19]. Being designed with algebraic manipulation software, all coefficients of this triplet are known with exact rational numbers. However, we mostly present double precision data in order to save space. The triplet **AP4o33vsi** (Adjoint Peer method with **4** stages, **orders** $q = 3$ for state and adjoint, **variable stepsizes**, **smooth grids**, **iteration**) is based on the nodes

$$\mathbf{c}^T = \left(\frac{144997}{389708}, \frac{73}{748}, \frac{77297572}{117896267}, 1 \right) \doteq (0.37207, 0.09759, 0.65564, 1). \quad (54)$$

The diagonal matrix K is also positive definite and, hence, preserves the sign in the cone condition (15). The triplet has a substantially larger angle $\alpha > 83^\circ$ of $A(\alpha)$ -stability than **AP4o33vgi** and the complement of its stability region is contained in $[-0.6, 20] \times [-15, 15]$. One drawback is larger error constants, see Table 1. The standard method is uniformly zero stable in $[\underline{\sigma}, \bar{\sigma}] = [0.65, 1.80]$ and it has LSRK form again, but not its adjoint method. For the adjoint method, we now have in condition (33) for super-convergence [19, Lemma 5.1],

$$\mathbb{1}^T A^T \beta_q^\dagger(\sigma) = \hat{a}_{s1}(1 - \sigma^q),$$

where $\hat{a}_{41} \leq 0.1011$ here. Hence, for **AP4o33vsi** it only holds that

$$\mathbb{1}^T A \beta_3(\sigma) = e_4^T \beta_3(\sigma) \equiv 0, \quad |\mathbb{1}^T A^T \beta_3^\dagger(\sigma_n)| = |\hat{a}_{41}(1 - \sigma^3)| \leq \frac{2}{3} |1 - \sigma| \leq \frac{2}{3} \eta h_n, \quad (55)$$

if $\sigma_n \in [\underline{\sigma}, \bar{\sigma}]$ and (34) are obeyed in the grid construction. The constant in (55) is computed from $\hat{a}_{41}(1 + \bar{\sigma} + \bar{\sigma}^2) \doteq 0.611 \leq 2/3$. This means that the adjoint method possesses global order for smooth grids only.

Since **AP4o33vsi** is not flip-symmetric, the boundary methods are independent. For both methods, optimization of the contraction factors was performed for each with the 4 free diagonals of \tilde{A}_0 resp. \tilde{A}_N and the 2 additional parameters from the boundary methods itself, see (41). The coefficients of these methods are given in Appendix A2. The contraction factors $\rho_{\mathbb{R}}$ on the real axis are again below $1/15$ and despite the much larger value of the stability angle $\alpha > 83^\circ$ also $\rho_{\alpha, N} \doteq 0.22$ may be acceptable while $\rho_{\alpha, 0} \cong 1/8$ is even smaller than for the pulcherrima triplet. Also the error constants of the boundary methods have a size similar to the standard method, see Table 2.

6.3 Global error estimates

Estimates for the global errors may be obtained by repeating the proof presented in [18] for uniform grids now for variable stepsizes using the weighted norm (25) constructed in the design process of the Peer triplets in [19]. Since its weight W is the same on the whole grid with fixed condition number $\|W\|_\infty \|W^{-1}\|_\infty$, the estimate carries over to the maximum norm of the global error. By a fixed point argument, the proof in [18] showed that the maximal global error on the

grid is bounded by the local errors in the form $3\|\mathbb{M}_0^{-1}\tau\|$, where the matrix \mathbb{M}_0 is a block matrix essentially containing the h -independent parts of the scheme. So, \mathbb{M}_0^{-1} mainly consists of products of the stability matrices $\bar{B}_n = A_n^{-1}B_n$ or $A_n^\top B_{n+1}^\top$ which all are bounded by one in the norm (25) or its adjoint equivalent. Collecting variables as $z^\top = (y^\top, p^\top, u^\top)$, $Z_n^\top = (Y_N^\top, P_n^\top, U_n^\top)$, etc., and abbreviating $f(z) := f(y, u)$, the fixed-point argument requires upper limits on the derivatives $\nabla_z f$, $(1 + \|z\|)\nabla_{zz} f$ in a tubular neighborhood of the exact solution z^* . Moreover, a stronger version of the control uniqueness property mentioned above requires upper limits for $\|(p^\top \nabla_{uu} f(z^*))^{-1}\|$ and $\|p^\top \nabla_{uzz} f(z)\|$ in the neighborhood.

Then, summing up the local errors in $\mathbb{M}_0^{-1}\tau$, the localized estimates from (28), (30) can be preserved. Since superconvergence eliminates the leading error not completely, the error bound will depend on two consecutive derivatives. The corresponding estimates will be abbreviated by a Matlab-type notation

$$\|\varphi^{(q:r)}\|_{[n]} := \max_{q \leq k \leq r} \|\varphi^{(k)}\|_{[n]}, \quad 0 \leq q \leq r, \quad 0 \leq n \leq N, \quad (56)$$

for sufficiently smooth functions $\varphi(t)$. Combining now the proofs of Lemma 6.1 in [19] and Lemma 7.1 from [18], the global error may be estimated by

$$\begin{aligned} & \max_{n=0}^N \{\|Y_n - \mathbf{y}_n\|_\infty, \|P_n - \mathbf{p}_n\|_\infty, \|U_n - \mathbf{u}_n\|_\infty\} \\ & \leq \mu \max_{n=0}^N h_n^{s-1} \max \{ \|(y^*)^{(s-1:s)}\|_{[n]}, \|(p^*)^{(s-1:s)}\|_{[n]}, \|(u^*)^{(s-1:s)}\|_{[n]} \}, \end{aligned} \quad (57)$$

where (57) holds for the pulcherrima triplet **AP4o33vgi** for general grids with bounded stepsize ratios $\sigma_n \in [\underline{\sigma}, \bar{\sigma}]$ due to (52), while for **AP4o33vsi** also smoothness $|\sigma_n - 1| \leq \eta h_n$ is required, see (55). We note that this error bound relates the local stepsize to the local size of solution derivatives as a justification for the kind of error control discussed in the next section.

7 A posteriori equi-distribution of global errors

In [19, Chapter 7.1.2], we have discussed the opportunity to provide an optimized stepsize sequence a priori using the exact solution $y(t)$ to implement an error equi-distribution principle introduced in [3, Chapter 9.1.1]. Here, we are going to exploit a posteriori error estimators to approximate global errors. Since the last row of the inverse of a Vandermonde matrix contains the coefficients of the highest difference expression, we set for our four-stage third-order Peer triplets

$$v_1^\top = 6e_4^\top V_4^{-1}, \quad v_2^\top = 6e_4^\top V_4^{-1} \mathcal{P}_4^{-1},$$

and define the estimators as a weighted mean of the polynomial derivatives from two intervals,

$$\varepsilon_0^Y = v_1^\top Y_0, \quad \varepsilon_n^Y = \delta v_1^\top Y_n + (1 - \delta) \sigma_n^{s-1} v_2^\top Y_{n-1}, \quad n = 1, \dots, N,$$

$$\varepsilon_N^P = v_1^\top P_N, \quad \varepsilon_{n-1}^P = (1 - \delta) v_1^\top P_n + \delta \sigma_n^{s-1} v_2^\top P_{n-1}, \quad n = 1, \dots, N.$$

where $\delta \in [0, 1]$ is chosen as a weighting factor. Taylor expansions with exact solutions $(y^*(t), p^*(t))$ at off-step points $t = t_{ni}$ yield $\varepsilon_n^Y = h_n^3 y^{*(3)}(t_n) + O(h_n^4)$ and $\varepsilon_n^P = h_n^3 p^{*(3)}(t_n) + O(h_n^4)$. Supposing an asymptotic behaviour of the global errors,

$$\|y(t_n) - Y(t_n)\| = O\left(h_n^3 \|y^{*(3)}(t_n)\|\right), \quad \|p(t_n) - P(t_n)\| = O\left(h_n^3 \|p^{*(3)}(t_n)\|\right)$$

with numerical approximations $Y(t_n) = e_1^\top V_4^{-1} Y_n$ and $P(t_n) = e_1^\top V_4^{-1} P_n$, the estimators defined above can be used to construct a new time mesh with nearly equally distributed global errors. In order to simplify equi-distribution of these errors, often linearized versions such as $h_n \|y^{*(3)}(t_n)\|^{1/3}$ and $h_n \|p^{*(3)}(t_n)\|^{1/3}$ are considered, see e.g. [14]. Defining the extended vector of approximate third derivatives $d_n := ((\varepsilon_n^Y)^\top, (\varepsilon_n^P)^\top)^\top / h_n^3$ and a piecewise constant mesh density function $\psi(t) := \|d_n\|^{1/3}$, $t \in [t_n, t_{n+1}]$, on the old grid it holds that

$$\int_{t_n}^{t_{n+1}} \psi(t) dt = h_n \psi(t_n) = h_n \|d_n\|^{1/3} \approx C (\|y(t_n) - Y(t_n)\|^2 + \|p(t_n) - P(t_n)\|^2)^{1/6}.$$

The equi-distribution of the global errors over a new mesh $0 < t'_1 < \dots < t'_{N+1} = T$ requires that

$$\int_{t'_n}^{t'_{n+1}} \psi(t) dt = \frac{1}{N+1} \int_0^T \psi(t) dt = \text{const}, \quad n = 0, \dots, N. \quad (58)$$

Since the global errors for the state and adjoint variables can differ by several orders of magnitude, we have to apply an appropriate weighting procedure to make sure that both errors are equally considered in the mesh design. Note that improving the approximate adjoints is a key to enhance the quality of the computed control. This motivates the definition of the following practical, component-wise weighted measures:

$$\begin{aligned} \theta_n^Y &:= \text{err}_{3,n} \max_{i=1,\dots,m} \frac{|\varepsilon_{ni}^Y|}{atol_Y + rtol_Y \hat{Y}_{ni}}, \quad n = 0, \dots, N, \\ \theta_n^P &:= \text{err}_{3,n}^\dagger \max_{i=1,\dots,m} \frac{|\varepsilon_{ni}^P|}{atol_P + rtol_P \hat{P}_{ni}}, \quad n = 0, \dots, N, \end{aligned}$$

with the intermediate values

$$\hat{Y}_0 = |Y(t_0)|, \quad \hat{Y}_n = \delta |Y(t_n)| + (1 - \delta) |Y(t_{n-1})|, \quad n = 1, \dots, N,$$

$$\hat{P}_N = |P(t_N)|, \quad \hat{P}_{n-1} = \delta |P(t_{n-1})| + (1 - \delta) |P(t_n)|, \quad n = 1, \dots, N,$$

and the individual error constants $\text{err}_{3,n}$, $\text{err}_{3,n}^\dagger$ from Table 1 and Table 2. Selecting appropriate values for the scaling parameters $atol_Y$, $atol_P$, $rtol_Y$, and $rtol_P$ is crucial and should reflect the nature of the problem. Defining the vector of the balanced weighted error estimators

$$\theta_n := ((\theta_n^Y)^\top, \omega(\theta_n^P)^\top)^\top, \quad \omega = \|\theta_n^Y\|_\infty / \|\theta_n^P\|_\infty,$$

we eventually define the mesh density function by $\psi(t) := \|\theta_n/h_n^3\|^{1/3}$, $t \in [t_n, t_{n+1}]$.

Then, an efficient way to construct a new mesh $0 = t'_0 < t'_1 < \dots < t'_{N+1} = T$ which distributes a given mesh density function $\psi(t) > 0$ evenly according to (58) is the computation of a smooth mesh function $x(\xi)$, $\xi \in [0, 1]$, which defines the grid through

$$t'_n = x(\xi_n), \quad \xi_n = \frac{n}{N+1}, \quad n = 0, \dots, N+1. \quad (59)$$

According to [14, Chapter 2.2.2] such a mesh function may be computed as the solution of the nonlinear boundary value problem

$$(\psi(x)x_\xi)_\xi = 0, \quad x(0) = 0, \quad x(1) = T, \quad (60)$$

where the lower index ξ denotes derivation. Since the full order of some Peer triplets requires that the used grids are smooth satisfying $\sigma_n = 1 + O(h_n)$, we will discuss now how the expression

$$\eta_n := \frac{\sigma_n - 1}{h_n} = \frac{h_n - h_{n-1}}{h_{n-1}h_n} \quad (61)$$

relates to the grid functions $x(\xi), \psi(t)$.

Lemma 7.1 *Let the grid $\{t'_n\}$ be defined according to (59) with some smooth mesh function $x(\xi)$, $h'_n := t'_{n+1} - t'_n$, and $\sigma'_n := h'_n/h'_{n-1}$. Then,*

$$\eta'_n = \frac{\sigma'_n - 1}{h'_n} = \frac{x_{\xi\xi}(\xi_n)}{(x_\xi(\xi_n))^2} + O\left(\frac{1}{(N+1)^2}\right). \quad (62)$$

If the mesh function $x(\xi)$ is the solution of the boundary value problem (60) with some smooth, positive density function ψ , then also

$$\eta'_n = -\frac{\psi'(t'_n)}{\psi(t'_n)} + O\left(\frac{1}{(N+1)^2}\right) = -(\ln \psi)'|_{t'_n} + O\left(\frac{1}{(N+1)^2}\right). \quad (63)$$

Proof. For ease of writing, we abbreviate $\delta := (N+1)^{-1}$.

a) Using Taylor expansion at ξ_n in (61), we get

$$\begin{aligned} h'_n - h'_{n-1} &= x(\xi_{n-1}) - 2x(\xi_n) + x(\xi_{n+1}) = \delta^2 x_{\xi\xi}(\xi_n) + \frac{\delta^4}{12} x^{(4)}, \\ h'_{n-1}h'_n &= \delta^2 (x_\xi(\xi_n))^2 + \frac{\delta^2}{12} (4x_\xi(\xi_n)x^{(3)} - 3x_{\xi\xi}(\xi_n)^2), \end{aligned}$$

where the highest derivatives are evaluated at some intermediate point. This shows (62).

b) The differential equation in (60) may also be written as $\psi x_{\xi\xi} + \psi' x_\xi^2 = 0$, which shows that $x_{\xi\xi}/x_\xi^2 = -\psi'/\psi$. \square

For the solution of (60), we use MMPDELab by W. Huang [13] and start with a uniform grid. Linear finite elements with N inner nodes ξ_n , $n = 1, \dots, N$, and a pseudo-timestepping scheme are applied. Additionally, we apply the smoothing of the mesh density function $\psi(t)$ in MMPDELab by controlling the ratios $\psi'(t'_n)/\psi(t'_n)$ from (63) in order to guarantee $\sigma'_n = 1 + \eta'_n h'_n$ with $|\eta'_n| \leq 15$ on the new mesh $t'_n = x(\xi_n)$. Such meshes yield smoothly varying stepsize sequences and work quite well for our variable stepsize Peer methods.

In what follows, we will apply this approach to two problems: (i) boundary control for the 1D heat equation with known exact discrete solutions [17] and (ii) optimal control of cytotoxic therapies on prostate cancer growth in 2D [8]. All calculations have been done with Matlab-Version R2019a on a Latitude 7280 with an i5-7300U Intel processor at 2.7 GHz.

8 Numerical results

8.1 Boundary control for the 1D Heat equation

The first problem, originally introduced in [17], was specifically constructed to yield exact analytical solutions for an optimal boundary control problem governed by a one-dimensional discrete heat

equation. The objective function evaluates both the deviation of the final state from a desired target and the cost of the control. Since there are no spatial discretization errors, the numerical convergence orders of time integration methods can be determined with high precision, without the need for a numerical reference solution.

The optimal control problem reads as follows:

$$\begin{aligned} & \text{minimize } \frac{1}{2} \|y(1) - \hat{y}\|_2^2 + \frac{1}{2} \int_0^1 u(t)^2 dt \\ & \text{subject to } y'(t) = Ay(t) + \gamma e_m u(t), \quad t \in (0, 1], \\ & \quad y(0) = \mathbb{1}_m, \end{aligned}$$

with

$$A = \frac{1}{(\Delta x)^2} \begin{pmatrix} -1 & 1 & & & \\ 1 & -2 & 1 & & \\ & \ddots & \ddots & \ddots & \\ & & 1 & -2 & 1 \\ & & & 1 & -3 \end{pmatrix},$$

state vector $y(t) \in \mathbb{R}^m$, $\Delta x = 1/m$, and $\gamma = 2/(\Delta x)^2$. We set $m = 250$. The components $y_i(t)$ approximate the solution of the continuous 1D heat equation $Y(x, t)$ over the spatial domain $[0, 1]$ at the discrete points $x_i = (i - 0.5)\Delta x$, $i = 1, \dots, m$. The corresponding boundary conditions are $\partial_x Y(0, t) = 0$ and $Y(1, t) = u(t)$. The matrix $A \in \mathbb{R}^{m \times m}$ results from standard central finite differences. Its eigenvalues λ_k and corresponding normalized orthogonal eigenvectors $v^{[k]}$ are given by

$$\begin{aligned} \lambda_k &= -4m^2 \sin^2 \left(\frac{\omega_k}{2m} \right), \quad \omega_k = \left(k - \frac{1}{2} \right) \pi, \\ v_i^{[k]} &= \nu_k \cos \left(\omega_k \frac{2i - 1}{2m} \right), \quad \nu_k = \frac{2}{\sqrt{2m + \sin(2\omega_k)/\sin(\omega_k/m)}}, \quad i, k = 1, \dots, m. \end{aligned}$$

Introducing an additional component $y_{m+1}(t)$ and adding the equations $y'_{m+1}(t) = u(t)^2$, $y_{m+1}(0) = 0$, the objective function can be transformed to the Mayer form

$$\mathcal{C}(y(1)) := \frac{1}{2} \left(\sum_{i=1}^m (y_i(1) - \hat{y}_i)^2 + y_{m+1}(1) \right)$$

with the extended vector $\bar{y}(1) = (y_1(1), \dots, y_m(1), y_{m+1}(1))^T$.

Following the test case in [17], we define the target vector \hat{y} through

$$\hat{y}(t) = y^*(T) - \delta (v^{[1]} + v^{[2]}).$$

with $\delta = 1/75$ and the exact solution $y^*(T) = \sum_{i=1, \dots, m} \eta_k(T) v^{[k]}$. The coefficients $\eta_k(T)$ are given by

$$\eta_k(T) = e^{\lambda_k T} \eta_k(0) - \gamma^2 \delta T v_m^{[k]} \sum_{l=1}^2 v_m^{[l]} \varphi_1((\lambda_k + \lambda_l)T)$$

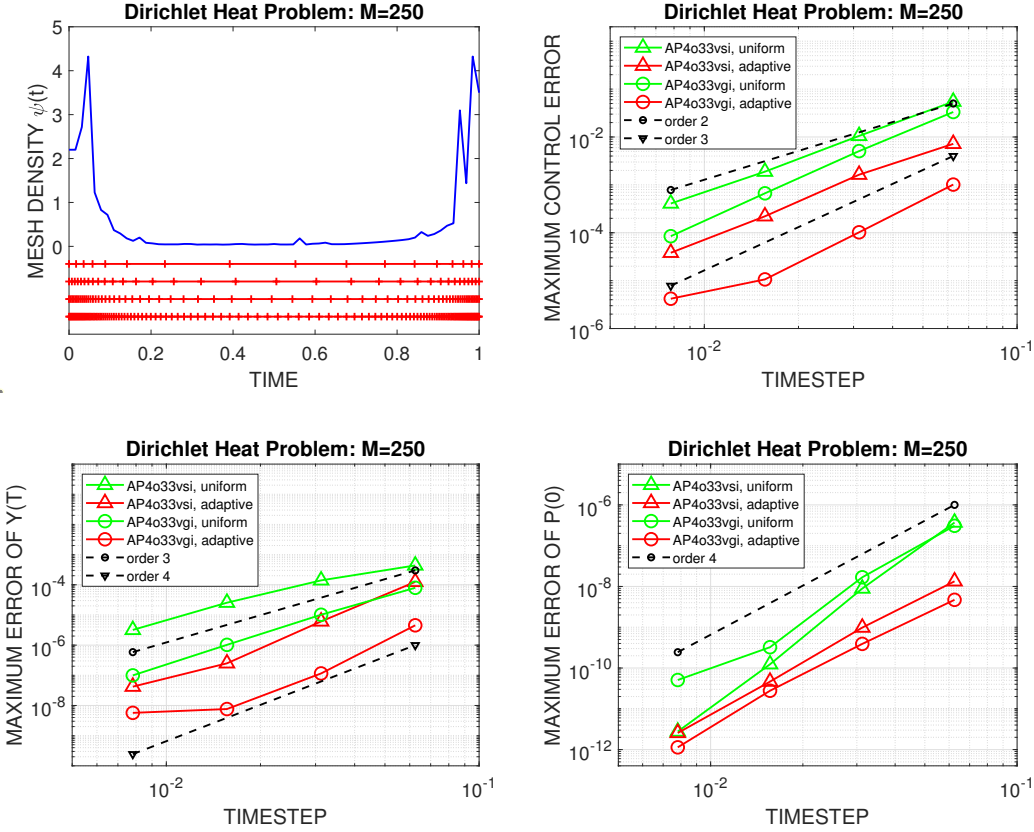


Figure 1: Dirichlet heat problem with $m = 250$ spatial points. Exemplary mesh density function $\psi(t)$ for AP4o33vgi, $N = 63$ and adapted time grids for $N = 15, 31, 63, 123$ (top left). Convergence of the maximal control errors $\|U_{ni} - u(t_{ni})\|_\infty$ (top right), state errors $\|y(T) - y_h(T)\|_\infty$ (bottom left), and adjoint errors $\|p(0) - p_h(0)\|_\infty$ (bottom right) for uniform and adaptive time grids.

where $\eta_k(0) = y^*(0)^\top v^{[k]}$ and $\varphi_1(z) := (e^z - 1)/z$. The exact control and adjoint are

$$u^*(t) = -\gamma p_m(t), \quad p^*(t) = \delta \left(e^{\lambda_1(T-t)} v^{[1]} + e^{\lambda_2(T-t)} v^{[2]} \right).$$

We will compare the numerical errors for $y(T)$, $p(0)$ and $u(t)$. An approximation $p_h(0)$ for the Peer method is obtained from $p_h(0) = e_1^\top V_4^{-1} P_0$. Note that, compared to [17], we have changed the sign of the adjoint variables, i.e., $p \mapsto -p$, to fit into our setting.

We performed calculations for $N + 1 = 16, 32, 64, 128$ with the results shown in Figure 1. The default interior-point algorithm in `fmincon` was used, with a zero control vector as the initial guess for uniform time grids. We set $\delta = 0$, $atol_Y = atol_P = 10^{-8}$, and $rtol_Y = rtol_P = 1$ to calculate the mesh density function. The self-adjoint method AP4o33vgi performs remarkably well, achieving average convergence orders of 3.2 for the state and 4.2 for the adjoint variables. This results in third-order convergence for the controls, even on coarse time grids. For variable-stepsizes, observed orders of convergence exceeding the expected ones may be explained by the fact that on fine grids

a disproportionate amount of points may be placed in the critical parts of the problem domain. The method **AP4o33vsi**, which offers a larger angle for $A(\alpha)$ -stability but has fewer symmetry properties, attains an asymptotic convergence order of 3 for the state and an unexpectedly high average of 5.7 for the adjoint. This yields an average convergence order of 2.4 for the control.

The mesh density function $\psi(t)$ reflects the expected behaviour for the linear heat equation. Larger, well-balanced global errors are observed at both ends of the time interval (see Figure 1, top left). Solving (60) using MMPDELab with smoothing yields improved variable time grids with significant refinements near the boundaries. The resulting meshes satisfy $\sigma_n = 1 + \eta_n h_n$ with $|\eta_n| \leq 15$. More precisely, we get

$$\min_n \sigma_n = \begin{cases} (0.69, 0.76, 0.87, 0.96) & \text{for AP4o33vgi,} \\ (0.65, 0.77, 0.88, 0.94) & \text{for AP4o33vsi,} \end{cases}$$

$$\max_n \sigma_n = \begin{cases} (1.75, 1.29, 1.15, 1.03) & \text{for AP4o33vgi,} \\ (1.33, 1.31, 1.14, 1.06) & \text{for AP4o33vsi.} \end{cases}$$

The improvement in control accuracy achieved by both methods is significant, approximately by a factor of 10 for **AP4o33vsi** and nearly 50 for **AP4o33vgi**, except at $N + 1 = 64$, where the improvement is somewhat lower. This clearly demonstrates the potential of using adaptive time grids and time integrators that maintain their order for such grids. In all cases, the post-processed control variables U_{ni}^\ddagger defined in (17) do not show a visible improvement and therefore do not contribute to a higher convergence order. As a result, we omit the details.

The triangular approximation at the boundaries, i.e., using \tilde{A}_i instead of A_i , $i = 0, N$, requires 10 – 15 iteration steps to meet a relative tolerance of 10^{-14} in the maximum norm for all smaller subsystems which are solved by the sparse direct solver of MATLAB. For practical tolerances as 10^{-6} , only 5 – 7 iteration steps are necessary, compared to one direct solve for the fully coupled (linear) system of fourfold size.

8.2 2D Prostate cancer growth

The second problem, taken from [8], addresses the optimal control of cytotoxic and antiangiogenic therapies in the treatment of prostate cancer (PCa). The mathematical model in a three-dimensional space-time cylinder $Q_T := \Omega \times (0, T)$ with boundary $\Sigma_T := \partial\Omega \times (0, T)$ reads as follows:

$$\partial_t \phi - \lambda \Delta \phi = -F'(\phi) + (m(\sigma) - U)h'(\phi) \quad \text{in } Q_T, \quad (64)$$

$$\partial_t \sigma - \eta \Delta \sigma = -\gamma_h \sigma - (\gamma_c - \gamma_h)\sigma\phi + S_h(1 - \phi) + (S_c - S)\phi \quad \text{in } Q_T, \quad (65)$$

$$\partial_t p - D \Delta p = -\gamma_p p + \alpha_h + (\alpha_c - \alpha_h)\phi \quad \text{in } Q_T, \quad (66)$$

with boundary and initial conditions

$$\phi = 0, \partial_n \sigma = \partial_n p = 0 \quad \text{in } \Sigma_T, \quad (67)$$

$$\phi(0, x) = \phi_0(x), \sigma(0, x) = \sigma_0(x), p(0, x) = p_0(x) \quad \text{in } \Omega. \quad (68)$$

Here, ϕ denotes the phase field variable that identifies the spatial location of the tumour, σ is the concentration of vital nutrients, and p is the tissue PSA concentration (prostate specific antigen).

The controls U and S describe the cytotoxic and antiangiogenic treatment effects, respectively. In the phase field equation it holds

$$F(\phi) = M\phi^2(1 - \phi)^2, \quad h(\phi) = M\phi^2(3 - 2\phi),$$

with mobility $M > 0$. The function $m(\sigma)$ is defined as

$$m(\sigma) = m_{ref} \left(\frac{\rho + A}{2} + \frac{\rho - A}{\pi} \arctan \left(\frac{\sigma - \sigma_l}{\sigma_r} \right) \right),$$

where $m_{ref} > 0$. A and ρ are constants that determine the rates of cell proliferation and cell death. We set $\rho = K_\rho/\bar{K}_\rho$ and $A = -K_A/\bar{K}_A$. The constants σ_l and σ_r are threshold and reference values for the nutrients, respectively. A characterization of all parameters and their values which are used in our computation are given in Appendix B.

The value for the clinically used serum PSA is determined from

$$P_s(t) = \int_{\Omega} p(t, x) dx.$$

Following [8], we define the two-dimensional simulation domain Ω as a square with edge length $l_d = 3000 \mu\text{m}$. The initial tumour is selected ellipsoidally in the centre of the domain:

$$\phi_0(x) = 0.5 - 0.5 \tanh \left(10 \left(\sqrt{\frac{(x_1 - l_d/2)^2}{a_1^2} + \frac{(x_2 - l_d/2)^2}{a_2^2}} - 1 \right) \right)$$

with $a_1 = 150 \mu\text{m}$ and $a_2 = 200 \mu\text{m}$. The initial values for the nutrients and PSA are estimated as

$$\sigma_0(x) = c_\sigma^0 + c_\sigma^1 \phi_0(x), \quad p_0(x) = c_p^0 + c_p^1 \phi_0(x)$$

with $c_\sigma^0 = 1 \text{ g/L}$, $c_\sigma^1 = -0.8 \text{ g/L}$, $c_p^0 = 0.0625 \text{ ng/mL/cm}^3$ and $c_p^1 = 0.7975 \text{ ng/mL/cm}^3$.

Initially the tumor growth is untreated for 60 days, i.e., $U(t) = 0$ and $S(t) = 0$. The results from [8] show that strong cytotoxic chemotherapy suffices to optimally control the volume and serum PSA of the tumor. So we also set $S(t) = 0$ for later times. The values of ϕ , σ , and p obtained at the end of the untreated growth phase are used as initial conditions for the optimal control problem with drug delivery. The time is reset to $t = 0$ and $T = 21$ days is used as a common duration of a therapy cycle for PCa.

The authors in [8] apply 256 isogeometric elements per side of the computational domain and a second-order time integrator with uniform stepsize $h = 0.1$ days to derive an optimal single cycle with smoothly decreasing $U_{d1}(t)$, starting with an initial guess $U_0(t) = m_{ref} \beta_c d_c e^{-t/\tau_c}$, where $\tau_c = 5$ days, $\beta_c = 1.59 \cdot 10^{-2} \text{ m}^2/\text{mg}$, $d_c = 75 \text{ mg/m}^2$ [8, Table 2]. The maximum value is set to $U_{max} = 0.12/\text{day}$, which corresponds to a 100 mg/m^2 drug dose of docetaxel. Running a nonlinear least-square fit of protocols in a post-processing treatment, a new 3-dose drug design of the form

$$U_{d3}(t) = \sum_{i=1}^3 m_{ref} \beta_c d_{c,i} e^{-\frac{t-t_{c,i}}{\tau_c}} H(t - t_{c,i})$$

has been proposed with $d_c = (58.49, 9.20, 5.03) \text{ mg/m}^2$, $t_c = (2.85, 7.90, 9.16) \text{ days}$ [8, Table 3], and H being the Heaviside function. The objective functional is given by

$$\begin{aligned} J(\phi, p, U) = & k_1 \int_{Q_T} \phi(t, x)^2 dx dt + k_2 \int_{\Omega} \phi(T, x)^2 dx \\ & + k_3 \int_0^T (P_s(t) - P_{\Omega})^2 dt + k_4 \int_{Q_T} (U - U_d)^2 dx dt, \end{aligned}$$

where $P_\Omega = \alpha_h |\Omega| / \gamma_c$, $U_d = 0$ and the weights were set to $k_1 = k_2 = k_3 = 1$, $k_4 = 0.5$. Note that $p(x, t) - \alpha_h / \gamma_c \geq 0$ due to $p_0(x) \geq \alpha_h / \gamma_p$ and $\phi(x, t) \geq 0$ in the model equations for p .

The use of a uniform stepsize of $h = 0.1$ days, which requests the numerical solution of 3650 systems of nonlinear equations with hundred thousands of spatial degrees of freedoms for each forward and backward run, and the two-step nature of the calculation of optimal controls is a serious limitation of the proposed algorithm. This becomes even more evident when drug protocols are to be designed for 3D PCa growth scenarios and longer simulation times are taken into account, reflecting conditions more closely aligned with experimental and clinical settings. A few numerical experiments with our third-order Peer triplets already showed that around 100 variable time steps are sufficient to reproduce the results above with acceptable accuracy. We now want to document this in detail.

Let $Z_m := \{x_i = (i - 0.5)\Delta x, i = 1, \dots, m\}$ be a set of discrete points lying in $[0, l_d]$. Then standard central differences of the diffusion terms and the homogeneous Neumann boundary conditions yield a second-order finite difference approximation $y(t)^\top := (\Phi(t)^\top, \Sigma(t)^\top, P(t)^\top) \in \mathbb{R}^{3m^2}$ of the PCa model equations on the two-dimensional grid $Z \times Z$ with long stacked space grid vectors $\Phi(t) \in \mathbb{R}^{m^2}$, etc. We use $m = 256$, that means $\Delta x = 11.72 \mu\text{m}$, which results in using 6 discrete points to approximate the interface defined by the distance between $\phi = 0.05$ and $\phi = 0.95$. Applying row-wise numbering of the spatial degrees of freedom, the spatial integrals of the objective functional are discretized by the second-order trapezoidal rule with a row vector of weights

$$W_{tp} = \frac{(\Delta x)^2}{4} (w_1, w_2, \dots, w_2, w_1) \in \mathbb{R}^{m^2},$$

where

$$w_1 = (1, 2, \dots, 2, 1) \in \mathbb{R}^m, \quad w_2 = (2, 4, \dots, 4, 2) \in \mathbb{R}^m.$$

Then the discrete objective functional reads

$$\begin{aligned} J_{\Delta x}(\Phi, P, U) = & k_1 \int_0^T W_{tp} \Phi(t)^2 dt + k_2 W_{tp} \Phi(T)^2 \\ & + k_3 \int_0^T \left(W_{tp} \left(P(t) - \frac{\alpha_h}{\gamma_p} \mathbb{1} \right) \right)^2 dt + k_4 \int_0^T W_{tp} \mathbb{1} (U(t) - U_d(t))^2 dt \end{aligned}$$

with $\mathbb{1} \in \mathbb{R}^{m^2}$. A transformation to Mayer form is done by introducing a further component y_{3m^2+1} that satisfies

$$\begin{aligned} y'_{3m^2+1}(t) = & k_1 W_{tp} \Phi(t)^2 + k_3 \left(W_{tp} \left(P(t) - \frac{\alpha_h}{\gamma_p} \mathbb{1} \right) \right)^2 + k_4 W_{tp} \mathbb{1} (U(t) - U_d(t))^2, \\ y_{3m^2+1}(0) = & 0. \end{aligned}$$

Eventually, we get the reduced discrete objective function

$$C(y(T)) = k_2 W_{tp} \left((y(T))_1^{m^2} \right)^2 + y_{3m^2+1}(T).$$

The admissible set of controls is $U_{ad} := \{U(t) \in \mathbb{R} : 0 \leq U(t) \leq U_{max}\}$. We solved the optimal control problem with `AP4o33vgi` using $N = 83$ time steps of variable size. The algorithm *trust-region-reflective* was applied as recommended large-scale solver for `fmincon`, where $U_0(t)$ was taken as initial guess. The scaling parameters for the calculation of the mesh density function were set to $atol_Y = 10^{-8}$, $atol_P = 10^2$, and $rtol_Y = rtol_P = 1$. Once again, we used $\delta = 0$.

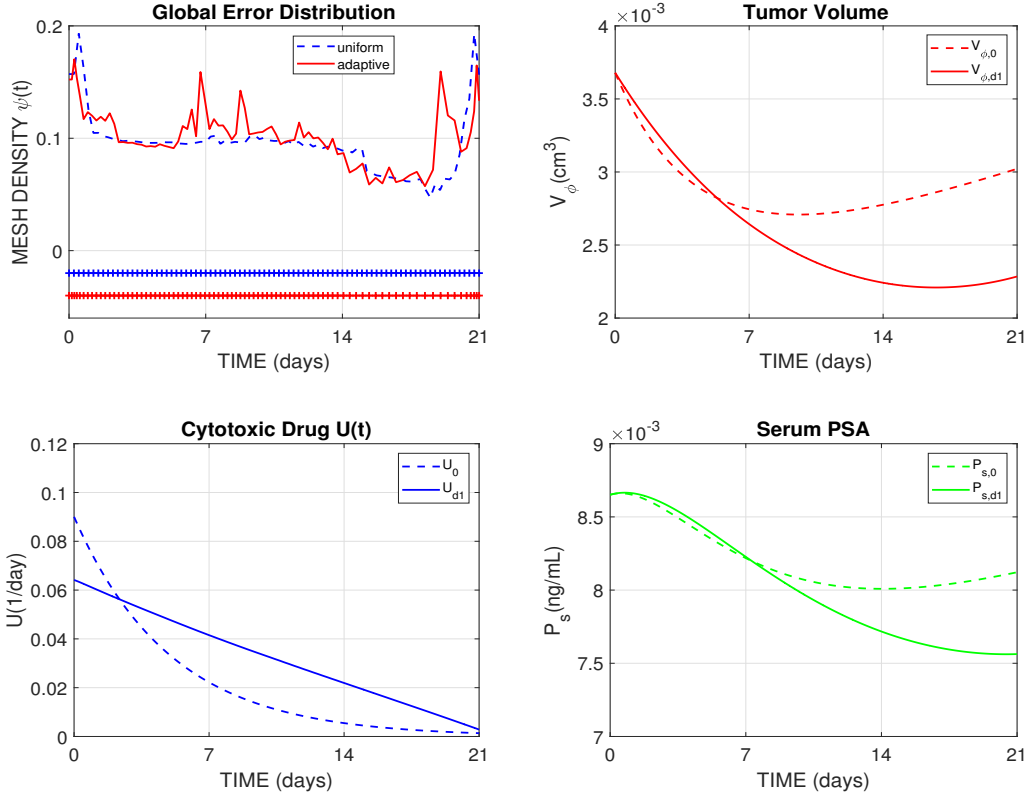


Figure 2: AP4o33vgi for PCa problem: single drug cycle. The target optimal cytotoxic 1-dose drug $U_{d1}(t)$ (bottom left) yields a significant smaller tumor volume $V_{\phi,d1}$ (top right) and serum PSA $P_{s,d1}$ (bottom right), compared to $V_{\phi,0}$ and $P_{s,0}$ obtained for the standard docetaxel protocol $U_0(t)$. Refining the time grid at both ends of the interval using the equi-distribution principle reduces the mesh density function there (top left) and leads to a reduction of the estimated maximum global error by nearly 40%. The measures of the adaptive mesh are $\sigma_n \in [0.75, 1.26]$ and $|\eta_n| \leq 2$.

Two different drug protocols were considered. In the first test, we reproduced the optimal single cycle with smoothly decreasing $U_{d1}(t)$ from [8] setting $U_d = 0$ in the objective function. Choosing $k_1 = k_2 = k_3 = 1$ and $k_4 = 6$, we achieved a good agreement with the results discussed in [8, Figure 4] with much fewer time steps. The results are presented in Figure 2. The `fmincon` solver converges in just 4 iterations, achieving 4-digit accuracy in the objective function within 27 minutes.

The second numerical study was concerned with the newly designed 3-dose drug protocol $U_{d3}(t)$ from above. Here, we set $U_d = U_{d3}$ in the objective function and investigated the evolution of the tumor volume and the serum PSA for different choices of the penalty parameter k_4 . In Figure 3, we summarize the results for $k_4 = 60$. A slight increase in the docetaxel doses improves the therapeutic result. Our algorithm is directly applicable, and the discontinuities in drug administration are resolved with sufficient accuracy. The quality of the computed gradients is remarkably high. So `fmincon` again achieves convergence in 4 iterations only, with 6-digit accuracy in the objective

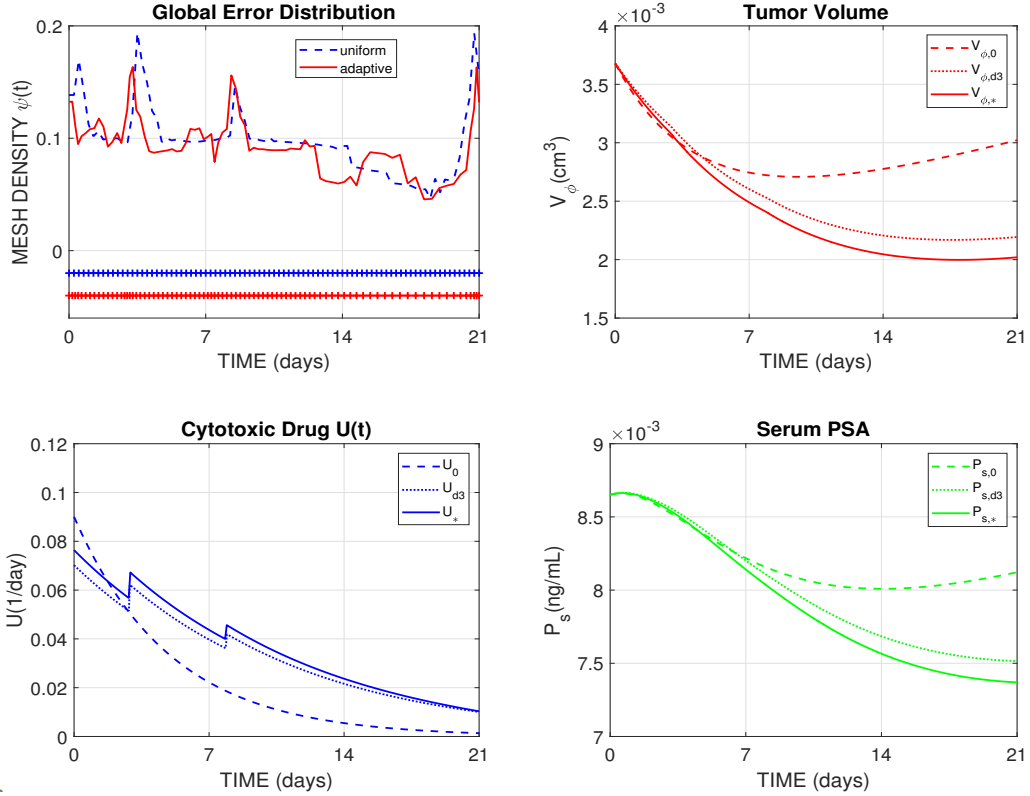


Figure 3: AP4o33vgi for PCa problem: 3-dose drug cycle. The numerical target optimal cytotoxic drug $U_*(t)$ (bottom left) yields a reduced tumor volume $V_{\phi,*}$ (top right) and serum PSA $P_{s,*}$ (bottom right), compared to $V_{\phi,d3}$ and $P_{s,d3}$ obtained for the 3-dose docetaxel protocol $U_{d3}(t)$. Refining the time grid at both ends of the interval and at the drug delivery time points t_c using the equi-distribution principle reduces the mesh density function in critical regions (top left) and leads to a reduction of the estimated maximum global error by 38%. The measures of the adaptive mesh are $\sigma_n \in [0.75, 1.20]$ and $|\eta_n| \leq 2$.

function. In both tests, the post-processed control variables U_{ni}^\ddagger do not improve the already high, third-order accuracy of the approximate controls.

By using triangular approximations at the boundaries, it is still possible to apply a sparse direct solver to linear systems of size 196,609. Typical iteration counts are around 12 for a relative tolerance of 10^{-3} , while approximately 6 iterations are typically required for the inner steps.

9 Conclusion

We modified two of the third-order Peer two-step triplets from [19] and integrated automatic grid construction in efficient gradient-based solution algorithms for the fully coupled optimal control problem with unknown control $u(t)$. Positivity of the quadrature weights in all matrices

K is essential. To avoid additional memory requirements in large nonlinear systems, special triangular iterations with small contraction factors are applied in the initial and final steps. Both schemes, **AP4o33vgi** and **AP4o33vsi**, perform very well on a benchmark problem involving boundary heat control — an application where one-step methods typically suffer from order reduction, as demonstrated in [17]. Noteworthy, the symmetry properties of the pulcherrima scheme **AP4o33vgi** yield increased orders between three and four for all components (y, u, p) , even on coarse grids.

As a second example, we applied our solution strategy to a real-world optimal control problem in medical treatment planning for prostate cancer, as discussed in [8]. In contrast to the main discretization parameters used in that work, our approach requires only 83 time steps of variable size — compared to 3650 for the generalized α -scheme — and just a few conjugate gradient steps using the large-scale optimization solver *trust-region-reflective* from MATLAB. This replaces the simpler *steepest-descent* gradient algorithm with step-size control and a fixed maximum of 100 iterations, while still achieving high-quality solutions. It also reflects the high-order consistency of the gradient provided by the self-adjoint **AP4o33vgi**. A further advantage is the opportunity to approximate optimal controls with steep gradients, allowing the direct study of alternative medical treatments close to real multi-dose drug protocols.

Summarizing, we believe that the two newly developed Peer two-step methods have the potential to significantly enhance the efficiency of solving large-scale optimal control problems. This includes applications such as designing effective drug protocols for 3D prostate cancer growth scenarios in clinical settings.

Acknowledgements. The first author is supported by the Deutsche Forschungsgemeinschaft (German Research Foundation) within the collaborative research center TRR154 “*Mathematical modeling, simulation and optimisation using the example of gas networks*” (Project-ID 239904186, TRR154/3-2022, TP B01).

A Coefficients of **AP4o33vgi** and **AP4o33vsi**

The essential data are the node vector $\mathbf{c}^\top = (c_1, c_2, c_3, c_4)$, the coefficients (A_0, K) , (A, K) , (A_N, K) of the starting, the standard and the end step and the free coefficients of the sparse matrix

$$\hat{B}(\sigma) = \begin{pmatrix} 1 & 1 & 1 & 1 \\ 0 & 0 & 0 & \hat{b}_{24}(\sigma) \\ 0 & 0 & 0 & \hat{b}_{34}(\sigma) \\ \hat{a}_{41} & \hat{b}_{42}(\sigma) & \hat{b}_{43}(\sigma) & \hat{b}_{44}(\sigma) \end{pmatrix},$$

depending on the stepsize ratio σ . All other coefficients may be computed by

$$a = A_0 \mathbf{1}, \quad w = A_N^\top \mathbf{1}, \quad B(\sigma) = V_4^{-\top} \hat{B}(\sigma) V_4,$$

where $V_4 = (\mathbf{1}, \mathbf{c}, \mathbf{c}^2, \mathbf{c}^3)$ is the Vandermonde matrix for the nodes in \mathbf{c} . Since the matrices A_0, A_N from the boundary steps are not in lower triangular form, we provide additional lower triangular approximations \tilde{A}_0, \tilde{A}_N to be used in fast Gauss-Seidel type block iterations (45) in order to avoid the solution of large coupled systems of fourfold size. Since the elements of \tilde{A}_0, \tilde{A}_N coincide with those of A_0, A_N in all subdiagonals, only the diagonals of \tilde{A}_0, \tilde{A}_N are given.

A1: Coefficients of AP4o33vgi

$$\begin{aligned}
\mathbf{c}^\top &= \left(0, \frac{1}{3}, \frac{2}{3}, 1\right), \quad K = \text{diag} \left(\frac{1}{8}, \frac{3}{8}, \frac{3}{8}, \frac{1}{8}\right), \\
A &= \begin{pmatrix} 1 & 0 & 0 & 0 \\ -\frac{9}{4} & \frac{9}{4} & 0 & 0 \\ \frac{9}{4} & -\frac{9}{2} & \frac{9}{4} & 0 \\ -1 & \frac{9}{4} & -\frac{9}{4} & 1 \end{pmatrix}, \quad \hat{B}(\sigma) = \begin{pmatrix} 1 & 1 & 1 & 1 \\ 0 & 0 & 0 & \frac{1}{36\sigma} \\ 0 & 0 & 0 & 0 \\ 0 & \frac{\sigma}{36} & \frac{\sigma}{18} & \frac{1}{804}(132\sigma + \frac{65}{\sigma} - 149) \end{pmatrix} \\
A_0 &= \begin{pmatrix} \frac{47161}{23112} & \frac{945}{1712} & \frac{9}{856} & -\frac{113}{1712} \\ -\frac{41383}{7704} & \frac{1017}{1712} & -\frac{27}{856} & \frac{339}{1712} \\ \frac{41383}{7704} & -\frac{4869}{1712} & \frac{1953}{856} & -\frac{339}{1712} \\ -\frac{47161}{23112} & \frac{2907}{1712} & -\frac{1935}{856} & \frac{1825}{1712} \end{pmatrix}, \quad A_N = \begin{pmatrix} \frac{1825}{1712} & -\frac{339}{1712} & \frac{339}{1712} & -\frac{113}{1712} \\ -\frac{1935}{856} & \frac{1953}{856} & -\frac{27}{856} & \frac{9}{856} \\ \frac{2907}{1712} & -\frac{4869}{1712} & \frac{1017}{1712} & \frac{945}{1712} \\ -\frac{47161}{23112} & \frac{41383}{7704} & -\frac{41383}{7704} & \frac{47161}{23112} \end{pmatrix}, \\
(\tilde{a}_{ii}^{(0)}) &= \left(\frac{154}{75}, \frac{69}{40}, \frac{219}{94}, \frac{67}{63}\right), \quad (\tilde{a}_{ii}^{(N)}) = \left(\frac{67}{63}, \frac{219}{94}, \frac{69}{40}, \frac{154}{75}\right).
\end{aligned}$$

A2: Coefficients of AP4o33vsi

$$\begin{aligned}
\mathbf{c}^\top &= \left(\frac{144997}{389708}, \frac{73}{748}, \frac{77297572}{117896267}, 1\right), \\
K &= \text{diag} (0.2089552772313791, 0.2461266069992848, 0.4259606950456414, 0.1189574207236947), \\
A_0 &= \begin{pmatrix} 1.26852968140859992 & -2.79702966259295784 & 0.0151774841161155076 & 0 \\ 0.254440961986028910 & 1.58797813851094452 & -0.00536671649536513773 & 0 \\ -3.75232398970999177 & 2.14140637287657549 & 2.46031830832026582 & 0 \\ 2.22935334631536294 & -0.932354848794562167 & -2.47012907594101619 & 1 \end{pmatrix}, \\
A &= \begin{pmatrix} 0.7588470158140062 & 0 & 0 & 0 \\ 0.4346633458753195 & 0.5989561692950702 & 0 & 0 \\ -3.295204661275873 & -0.3671669165116753 & 2.473930545531403 & 0 \\ 2.101694299586548 & -0.2317892527833949 & -2.473930545531403 & 1 \end{pmatrix}, \\
A_N &= \begin{pmatrix} 0.721680741868241430 & 0.0131418918926231641 & 0.03333333333333333333 & -0.00930895128019174555 \\ 0.123032993110224916 & 0.709147801969229717 & 0.279492058866634697 & -0.078053338775699573 \\ -1.03159221459763137 & -1.16757403034966595 & 0.443763401719389714 & 0.566961810971761768 \\ 5.56340552222272135 & -1.45584078718664692 & -5.57863709363081650 & 1.86704685986649197 \end{pmatrix}, \\
(\tilde{a}_{ii}^{(0)}) &= (1.58950617283950617, 1.66216216216216216, 2.47, 1), \\
(\tilde{a}_{ii}^{(N)}) &= (0.725, 0.6818181818181818, 2, 1.91525423728813559),
\end{aligned}$$

$$\hat{b}_{24} = 0.02321239244678227/\sigma, \quad \hat{b}_{34} = 0,$$

$$\hat{a}_{41} = 0.1010743874247749, \quad \hat{b}_{42} = \hat{a}_{41} + 0.003586671392069201 \sigma,$$

$$\hat{b}_{43} = \hat{a}_{41} + 0.007173342784138403 \sigma - 0.002465255918355442 \sigma^2,$$

$$\hat{b}_{44} = 0.0078782707622298066 + 0.1683589306029579 \sigma - 0.1125 \sigma^2 + 0.025 \sigma^3,$$

B: Model parameters for prostate cancer growth

Parameter	Notation	Value
Tumor dynamics		
Diffusivity of the tumor phase field	λ	$640 \mu\text{m}^2/\text{day}$
Tumor mobility	M	$2.5/\text{day}$
Net proliferation scaling factor	m_{ref}	$7.55 10^{-2}/\text{day}$
Scaling reference for proliferation rate	\bar{K}_p	$1.50 10^{-2}/\text{day}$
Proliferation rate	K_p	$1.50 10^{-2}/\text{day}$
Scaling reference for apoptosis rate	\bar{K}_A	$2.10 10^{-2}/\text{day}$
Apoptosis rate	K_A	$1.37 10^{-2}/\text{day}$
Nutrient dynamics		
Nutrient diffusivity	η	$6.4 10^4 \mu\text{m}^2/\text{day}$
Nutrient supply in healthy tissue	S_h	2 g/L/day
Nutrient supply in tumor tissue	S_c	2.75 g/L/day
Nutrient uptake by healthy tissue	γ_h	2 g/L/day
Nutrient uptake by tumor tissue	γ_c	17 g/L/day
Hypoxic-viable threshold for nutrients	σ_l	0.4 g/L
Scaling reference for nutrients	σ_r	$6.67 10^{-2} \text{ g/L}$
Tissue PSA dynamics		
Tissue PSA diffusivity	D	$640 \mu\text{m}^2/\text{day}$
Healthy tissue PSA production rate	α_h	$1.712 10^{-2} \text{ ng/mL/cm}^3/\text{day}$
Tumoral tissue PSA production rate	α_c	$\alpha_c = 15\alpha_h$
Tissue PSA natural decay rate	γ_p	$0.274/\text{day}$

References

- [1] G. Albi, M. Herty, and L. Pareschi. Linear multistep methods for optimal control problems and applications to hyperbolic relaxation systems. *Applied Mathematics and Computation*, 354:460–477, 2019.
- [2] I. Almuslimani and G. Vilmart. Explicit stabilized integrators for stiff optimal control problems. *SIAM J. Sci. Comput.*, 43:A721–A743, 2021.
- [3] U.M. Ascher, R.M.M. Mattheij, and R.D. Russell. *Numerical Solution of Boundary Value Problems for Ordinary Differential Equations*. Society for Industrial and Applied Mathematics, 1995.
- [4] D. Beigel, M.S. Mommer, L. Wirsching, and H.G. Bock. Approximation of weak adjoints by reverse automatic differentiation of BDF methods. *Numer. Math.*, 126:383–412, 2014.
- [5] F.J. Bonnans and J. Laurent-Varin. Computation of order conditions for symplectic partitioned Runge-Kutta schemes with application to optimal control. *Numer. Math.*, 103:1–10, 2006.
- [6] R.H. Byrd, J.C. Gilbert, and J. Nocedal. A trust region method based on interior point techniques for nonlinear programming. *Math. Program.*, 89:149–185, 2000.

- [7] T.F. Coleman and Y. Li. On the convergence of reflective Newton methods for large-scale nonlinear minimization subject to bounds. *Math. Program.*, 67:189–224, 1994.
- [8] P. Colli, H. Gomez, G. Lorenzo, G. Marinoschi, A. Reali, and E. Rocca. Optimal control of cytotoxic and antiangiogenic therapies on prostate cancer growth. *Math. Models Methods in Appl. Sci.*, 31:1419–1468, 2021.
- [9] W.W. Hager. Runge-Kutta methods in optimal control and the transformed adjoint system. *Numer. Math.*, 87:247–282, 2000.
- [10] W.W. Hager and R. Rostamian. Optimal coatings, bang-bang controls, and gradient techniques. *Optimal Control Applications and Methods*, 8:1–20, 1987.
- [11] E. Hairer, G. Wanner, and Ch. Lubich. *Geometric Numerical Integration, Structure-Preserving Algorithms for Ordinary Differential Equations*, volume 31 of *Springer Series in Computational Mathematic*. Springer, Heidelberg, Berlin, 1970.
- [12] M. Herty, L. Pareschi, and S. Steffensen. Implicit-explicit Runge-Kutta schemes for numerical discretization of optimal control problems. *SIAM J. Numer. Anal.*, 51:1875–1899, 2013.
- [13] W. Huang. *MMPDElab*, <https://github.com/weizhanghuang/MMPDElab>, 2019.
- [14] W. Huang and R.D. Russell. *Adaptive Moving Mesh Methods*. Springer New York, Dordrecht, Heidelberg, London, 2011.
- [15] J. Lang and B.A. Schmitt. Discrete adjoint implicit peer methods in optimal control. *J. Comput. Appl. Math.*, 416:114596, 2022.
- [16] J. Lang and B.A. Schmitt. Implicit A-stable peer triplets for ODE constrained optimal control problems. *Algorithms*, 15:310, 2022.
- [17] J. Lang and B.A. Schmitt. Exact discrete solutions of boundary control problems for the 1D heat equation. *J. Optim. Theory Appl.*, 196:1106–1118, 2023.
- [18] J. Lang and B.A. Schmitt. Implicit peer triplets in gradient-based solution algorithms for ODE constrained optimal control. *J. Optim. Theory Appl.*, 203:985–1026, 2024.
- [19] J. Lang and B.A. Schmitt. Variable-stepsize implicit peer triplets in ODE constrained optimal control. *J. Comput. Appl. Math.*, 460:116417, 2025.
- [20] J. Lang and J.G. Verwer. W-methods in optimal control. *Numer. Math.*, 124:337–360, 2013.
- [21] X. Liu and J. Frank. Symplectic Runge-Kutta discretization of a regularized forward-backward sweep iteration for optimal control problems. *J. Comput. Appl. Math.*, 383:113133, 2021.
- [22] J.M. Sanz-Serna. Symplectic Runge–Kutta schemes for adjoint equations, automatic differentiation, optimal control, and more. *SIAM Review*, 58:3–33, 2016.
- [23] P. Spellucci. An SQP method for general nonlinear programs using only equality constrained subproblems. *Math. Program.*, 82:413–448, 1998.
- [24] J.L. Troutman. *Variational Calculus and Optimal Control*. Springer, New York, 1996.